# A THEORETICAL STUDY OF METAL OXIDES

**ZAINAB NASIR**

**DEPARTMENT OF PHYSICS**

**KINNAIRD COLLEGE FOR WOMEN,**

**LAHORE, PAKISTAN**

**2022**

# A THEORETICAL STUDY OF METAL OXIDES

**A RESEARCH REPORT SUBMITTED TO**
**KINNAIRD COLLEGE FOR WOMEN**
**IN FULFILMENT OF THE REQUIREMENTS**
**FOR THE DEGREE OF**

**BACHELORS OF SCIENCE**
**IN**
**PHYSICS**

BY

**ZAINAB NASIR**

**DEPARTMENT OF PHYSICS**
**KINNAIRD COLLEGE FOR WOMEN, LAHORE**
**2022**

# RESEARCH COMPLETION CERTIFICATE

It is certified that **Ms. Zainab Nasir** of BS (session 2018-2022), Department of Physics has carried out research work entitled **"A Theoretical Study of Metal Oxides"** under my supervision.

It is assured that research work is original and has not yet been published anywhere else.

**Supervisor:**

Dated: 22-06-2022

**Aysha Aftab**

Lecturer in Physics
Kinnaird College for Women, Lahore.

**Head of Department:**

**Samia Maqsood**

Assistant Professor of Physics
Kinnaird College for Women, Lahore.

"All changes suggested by examiners during defense are incorporated in this final copy."

| Student | Supervisor | Head of Department |
|---|---|---|

# ANTI-PLAGIARISM DECLARATION

I certify that this is my own research work. The work has not, in whole or in part, been presented elsewhere for assessment. Where material has been used from other sources, it has been properly acknowledged. The similarity index of the research report is **12%**. If this statement is untrue and I am found guilty of plagiarism, the punitive action against me should be taken as per Kinnaird Anti Plagiarism Policy.

**Zainab Nasir**

Registration No: F18BPHY007

Program: BS PHYSICS

Signature: 

**Supervisor:**

**Aysha Aftab**

Lecturer in Physics
Kinnaird College for Women, Lahore.

**Head of Department:**

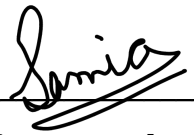

**Samia Maqsood**

Assistant Professor of Physics
Kinnaird College for Women, Lahore.

# ACKNOWLEDGEMENTS

In the name of Allah, the most gracious and the most merciful. All respect and praises to the Holy Prophet Hazrat Muhammad. May Allah send His Grace, honor and mercy upon our Lord, Hazrat Muhammad and upon his family! Verily, Allah is all knowing and Holy Prophet Muhammad is the light of knowledge for all the humanity. This thesis become a reality with the kind support and help of many individuals. I would like extend my sincere thanks to all of them. I humble acknowledge the constant support of my parents, siblings and mentors in completion of my thesis and degree successfully. I also like to submit my sincere gratitude to our Honorable Principal of Kinnaird College for Women Dr. Rukhsana David and Vice Principal Dr. Nikhat Khan for promoting research in science at all levels. My heartiest gratitude to the Head of Physics Department Ms. Samia Maqsood for her guidance and help. Further, I would like to mention Ms. Aysha Aftab, supervisor who gave me insightful feedback, guidance and co-operation throughout my research work. It was a great privilege and honor to work under her instruction. I express my deep sense of gratitude to all of my teachers and the staff of physics department who have helped me in various aspects of my thesis and throughout my degree. I am forever in debt to Kinnaird College for Women for providing me the platform and progressive environment needed for completion of my studies and research work. May I be able to fulfil my scientific dream in future! I would like to complete my acknowledgement on these words “The world belongs to the brave!” may Allah bless all of us! Ameen.

**Zainab Nasir**

# ABSTRACT

Crystallographic characteristics of different materials such as $ZrO_2$ and $\alpha$-$Fe_2O_3$ was theoretically analyzed. Modeling is the modern field of physics. Modeling comes in action for such conditions when it is either difficult or impossible to perform experiments and achieve particular conditions. Instead of directly performing experiments and taking measurements modeling is used as replacement. The goal of theoretical modelling is to make a particular aspect or an entire behavior of experimental evidences easier to grasp, characterize, simulate and visualize with eventually being able to forecast such behavior through the use of changing parameters. Transition metal oxide-based nanomaterials such as ZnO, $Co_3O_4$, $RuO_2$, $Fe_2O_3$, $ZrO_2$, $MnO_2$, $IrO_2$, $V_2O_5$, $WO_3$ and $In_2O_3$ have attracted a lot of attention due to their capacity to interact with atoms, molecules and ions not just at their active surfaces but also throughout the material. In this research, metal oxide-based nanomaterials polymorphs $ZrO_2$ and $\alpha$-$Fe_2O_3$ crystal structures models were created such as wireframe, polyhedral, stick and space filling for enhanced perception by using VESTA software. VESTA tool is used to visualize fractional coordinates for $\alpha$-$Fe_2O_3$ and $ZrO_2$. By using VESTA software powder diffraction pattern (XRD) were also formed and gives most intense lattice planes (111) and (104) for $ZrO_2$ and $\alpha$-$Fe_2O_3$ respectively. Calculated bond length of zirconium Zr with oxygen O1 and O2 is 2.1070 Å and 2.2634 Å sequentially while on the other hand bond length between Iron Fe and oxygen O is 1.5400 Å. The bond length is calculated in angstrom. These transition metal oxide-based nanomaterials are used in the field of security, energy and environment.

# A THEORETICAL STUDY OF METAL OXIDES

## TABLE OF CONTENTS

# LIST OF FIGURES

# LIST OF TABLES

# ABBREVIATIONS

| | |
|---|---|
| 3D | Three Dimensional |
| bcc | body-centered cubic |
| fcc | face-centered cubic |
| TMO’s | Transition metal oxides |
| MOs | metal oxides |
| ccp | cubic closed packed |
| hcp | hexagonal closed packed |
| XRD | X-ray diffraction |
| $\theta$ | Angle |
| $\lambda$ | Wavelength |
| n | Integer |
| VESTA | Visualization for Electronic and Structural Analysis |
| $d_{hkl}$ | spacing d between adjacent (h k l) |
| UV | Ultraviolet |
| PF | phenol formaldehyde |

# CHAPTER 1

# INTRODUCTION

## 1.1 Crystal Structures

Crystal structure is essentially a description of an organized arrangement of atoms, ions, and molecules in a crystalline substance in crystallography. These organized structures arose from the inherent nature of constituent particles to form symmetric patterns that will recur along with the primary directions of three-dimensional (3D) space in matter. These crystal structures describe the internal organization of atoms, ions, particles, and molecules and have nothing to do with the exterior look of any crystal. These crystal formations, on the other hand, are not totally autonomous. Many physical characteristics, like as cleavage, optical transparency, and electronic band structure, are determined by crystal structure and symmetry [1,2].

### 1.1.1 Unit Cell

Crystal structures are defined as the geometry of atoms, molecules, and particles arranged in a unit cell. It is described as the smallest collection of particles in any substance that creates this repeating pattern. A unit cell can reflect the full crystal structure and symmetry; a crystal is built by repetitive translation of a unit cell and its primary axes. The geometry of the unit cell may be characterized as a parallelepiped with six lattice parameters interpreted as cell edge lengths (a, b, c). ($\alpha$, $\beta$, $\gamma$) are denoted by the angles between them. The locations of particles inside a unit cell measured from a reference point are explained by fractional coordinates ($x_i$, $y_i$, $z_i$) along the cell boundaries. A crystal structure's space component is formed as a set of unit cell crystal symmetry [1].

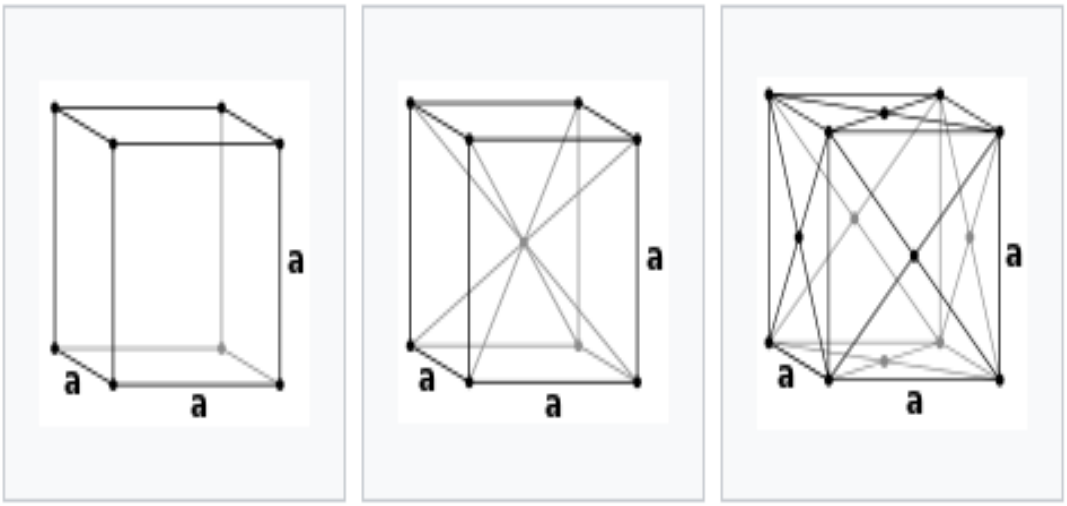


Figure 1.1 Shows the unit cell of simple cubic, body-centered cubic bcc and face-centered cubic fcc [1].

### 1.1.2 Lattice System

Lattice systems are described as a collection of crystal structures classified according to the axial system to characterize their lattice. Every lattice system contains a set having three axes, in particular geometric arrangement. The simple and most symmetric lattice system is the cubic or isometric system. There are six more lattice systems that includes hexagonal, triclinic, tetragonal, orthorhombic and monoclinic [1].

### 1.1.3 Bravais Lattice

Bravais lattices are defined as geometric configurations of lattice points with structural translational symmetries. There are Fourteen distinct Bravais lattices in the three dimensions of space, which explains translational symmetries. The Bravais lattice is regarded as the fundamental core component from which all crystals may be built. These lattices are embedded in 7 distinct crystal systems, which are distinguished by the linkage between the angles, the sides of the unit cell, and the length in between points of the unit cell [1,2].

### 1.1.4 Miller Indices

The three-value Miller index system can be used to define axes and planar in a lattice structure. The indices l, m, and n are used for directional parameters in the syntax. This syntax (l m n) denotes a plane. Miller indices typically equal to the inverse of plane intercepts, with the unit cell being the origin of the lattice vector. If one or more of the indices is 0, the planes will not intersect that axis. Negative indices are denoted by a horizontal bar on the digits [1].

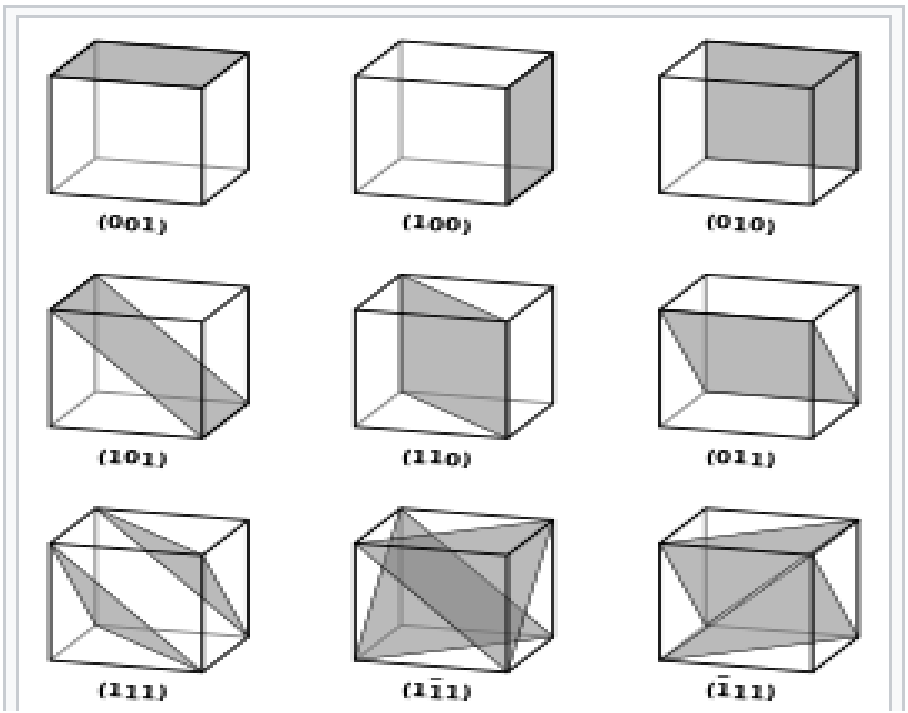


Figure 1.2 Planes in a unit cell with varying miller indices [1].

### 1.1.5 Description of Crystal Structure

There are number of ways by which crystal structures can be described. Its most typical method is to specify the size and form of the unit cell, as well as the locations of the atoms or ions inside the cell. This knowledge is often insufficient for interpreting the three-dimensional structure. Analysis of numerous unit cells, the organization of the atoms, ions, and molecules with regard to one another, the number of other atoms in contact with atoms, and distance to adjacent atom are all required for a deeper comprehension of a crystal structure. There are several approaches for describing extended solid state structures [2].

## 1.2 Metal Oxides

Metal oxides are basically crystalline solids that have a metal cation and oxide anion. Polymeric structure is adopted by most of metal oxides. Transition metal oxides (TMO's) are compounds that are composed of oxygen atoms to bound with transition metals. Following are the oxide-based nanomaterials of metallic elements such as $IrO_2$, $RuO_2$, $V_2O_5$, $MnO_2$, $WO_3$, $Fe_2O_3$, ZnO and $In_2O_3$ have gotten considerable attention from technological world due to its capability to converse with atoms, ions, and compounds conveniently, not only at their energetic outer surface but all over the substance. Metal oxides are being considered for a key part in the growth of renewable energy techniques and materials that meet the world's energy needs. In place of metal oxides MOs, transition metal oxides (TMOs) having general formula $MO_2$ are very significant nanomaterials. The formation of structural alterations is caused by polymorphic transformations in the binary metal oxides, which result in distinct polymorphs in the metal oxides like $TiO_2$, $ZrO_2$, $WO_3$, $Cr_2O_3$, $Fe_2O_3$, $MoO_3$ etc [3,4].

## 1.3 Presence of Elements in Periodic Table

The periodic table is regarded as a tabular representation of elements. The periodic table is divided into four rectangular areas called blocks that are s, p, d and f blocks. In periodic table rows are considered as periods while the columns in table are known as groups. Elements associated from a same column group, exhibit similar chemical characteristics. In a table, trend goes through with non-metallic character increasing throughout a period, it moves from left to right and across a group it moves from down to up. Metallic nature will increase in the opposite direction. There are 118 elements known out of which first 94 elements occur in nature and other elements are artificially created [5].

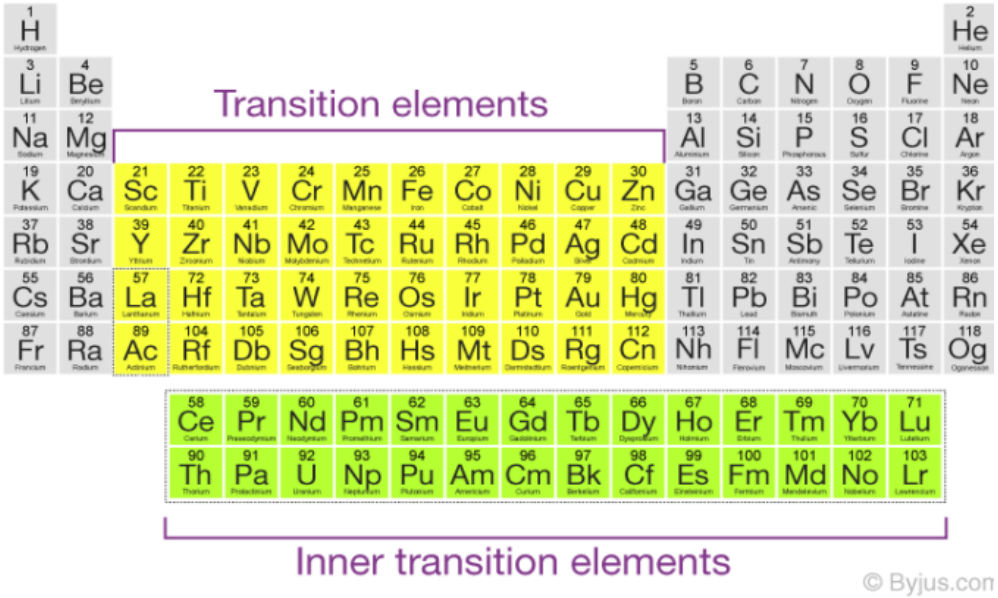


Figure 1.3 Illustrate the elements in periodic table [6].

### 1.3.1 D-Block Elements

D-block elements included in the contemporary periodic table found from 3rd group to 12th group of elements. Transition elements and transitions metals are also known as D-block elements. Members of group (1-10) contain electrons in the d-orbital, whereas d block elements are found in the outermost 's' orbital (1-2). In addition, the 12th group electrons never complete the 'd' orbital. But they are similar in many aspects to that of other groups elements of d-block. The reason for requesting d-block elements as transition elements is their location and transfer of properties between s and p block components. We can state that all transition elements or metals are d-block elements, however all d-block elements really aren't transition elements [6].

### 1.3.2 Properties of Transition Metals

Following are the properties of transitions metals

- Transitions elements shows metallic qualities for example malleability, ductility, heat capacity, high electrical absorption levels, and tensile strength.
- They are found in the periodic table between the 's' and 'p' block elements.

- Their attributes are shared by s and p block elements [6].

### 1.3.3 Metallic Character

D-block elements also shows metallic behavior and in contrast to s-block elements such as metallic elements and alkali metals, they get a strong binding energy. They exhibit excellent tensile properties, ductile, high thermal stability, malleability, metal luster, and therefore can crystalline in body-centered cells (bcc), cubic closed packed (ccp) cells, and hexagonal closed packed (hcp) cells. These metals consist of considerable mechanical strength especially in alloys. Effective metallic bonding exists between delocalized electrons in nearby electrons' outermost d orbitals, resulting in greater melting and boiling temperatures [6,7].

### 1.3.4 Classification of D block elements into four series

There have been four sets in the d block that can be used to fill 3,4,5,6-d orbitals. Every set has ten components that occupy the 'd' orbital. And they are as described in the following:

- Elements in the 3d-series include Sc, Ti, V, Cr, Mn, Fe, Co, Ni, Cu, and Zn.
- Elements in the 4d-series include Y, Zr, Nb, Mo, Tc, Ru, Rh, Pd, Ag, and Cd.
- The 5d-series comprises the elements La, Hf, Ta, W, Re, Os, Ir, Pt, Au, and Hg.
- The 6d-series is unfinished [6].

## 1.4 Polymorphism

Polymorphism is derived from a Greek term. It depends on mostly two terms “ Polus” and “Morph”. “Polus” means “many” while on other hand the term “morph” represent “shapes”. Polymorphism is an abbreviation meaning "many shapes." Polymorphism refers to a solid material's capacity to exist in much more than one state, whether it be in crystal structure or even in phases, and to have varied configurations and conformations of atoms in the crystalline lattice. Polymorphs are substances who have the same composition but a distinctive crystal structure [3].

## 1.5 Iron oxide $Fe_2O_3$

Iron Fe derived from the Latin word ferrum having the atomic weight 26. Iron is a metallic material that belongs to the periodic table's first transition series and group eight. It is classified as ferrite and seems to have a body-centered cubic bcc crystal structure. It's a soft metal that would also be thermally stable. At high temperatures, α-iron is magnetically paramagnetic. Previously, the paramagnetic state of α-iron was referred to as β-Fe; however, a tiny tetragonal deformation that occurs in the ferromagnetic state results in a real phase change.

Iron(III) oxide, sometimes known as ferric oxide, is a kind of inorganic chemical with the composition $Fe_2O_3$. It is among the three major oxides of iron, the other two being (FeO), which is uncommon, and iron(II,III) oxide $Fe_3O_4$, which may also persist in the environment as crystalline magnetite. The most prevalent type of iron is α-$Fe_2O_3$, which has a hexagonal structure [8,9,10].

## 1.6 Polymorph $Fe_2O_3$

$Fe_2O_3$ is often recognized as Iron Oxide, and it can be typically found as the minerals hematite. It is a significant source of iron for the steel manufacturing industry. $Fe_2O_3$ is a ferromagnetic, dark red material that is rapidly damaged by acidic chemicals. $Fe_2O_3$ exists in four major polymorphs [11]:

- α-$Fe_2O_3$
- γ-$Fe_2O_3$
- β-$Fe_2O_3$
- ε-$Fe_2O_3$

### 1.6.1 α-$Fe_2O_3$

α-$Fe_2O_3$ have rhombohedral crystalline structure the most prevalent configuration. This becomes an anti-ferromagnetic below 260 K temperature. It is found in nature as that of minerals hematite, which is exploited as basic iron ore [11].

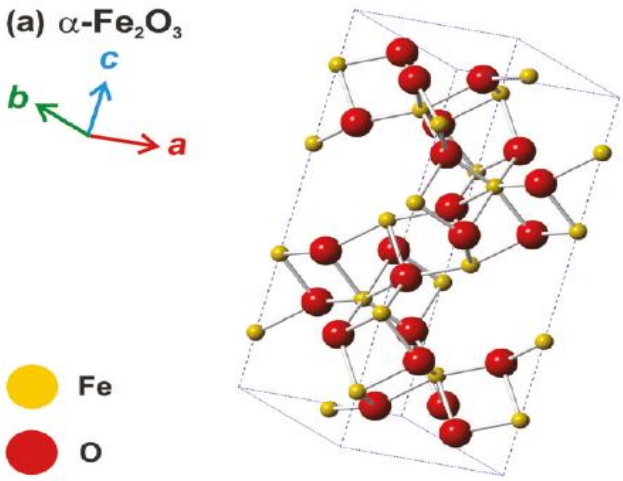


Figure1.4 Graphical representation of α-$Fe_2O_3$ [12].

### 1.6.2 γ-$Fe_2O_3$

The cubic crystal structure of γ-$Fe_2O_3$ persists in a metastable condition and is transformed from the γ-$Fe_2O_3$ phases at high temperatures. That's a ferromagnetic material that may be used in audio cassettes [11].

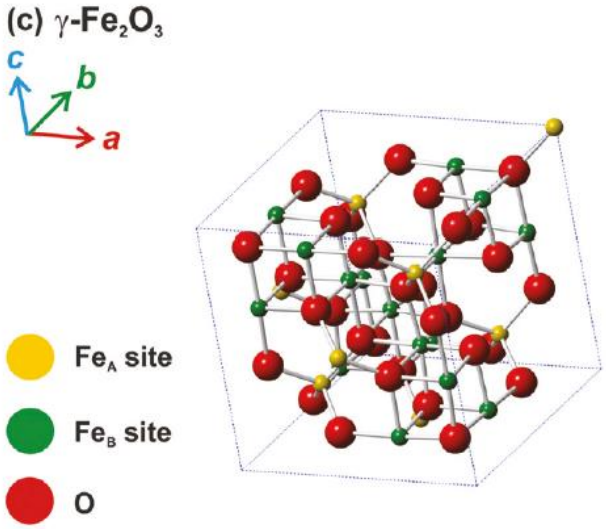


Figure 1.5 Graphical representation of γ-$Fe_2O_3$ [12].

### 1.6.3 β-$Fe_2O_3$

The β-$Fe_2O_3$ phases are body cubic centered bcc metastable and changes to the α-$Fe_2O_3$ phases at temperatures greater than 773 K. This can also be made by reducing hematite with thermal breakdown of iron sulphate [11].

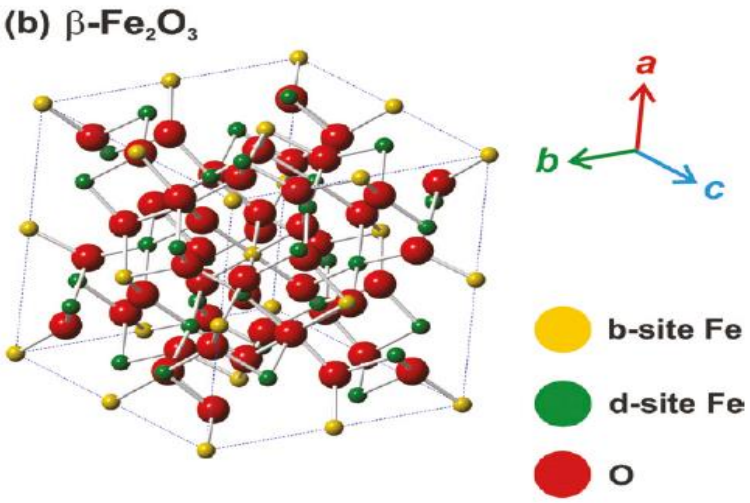


Figure 1.6 Graphical representation of β-$Fe_2O_3$ [12].

### 1.6.4 ε-$Fe_2O_3$

The ε-$Fe_2O_3$ phase seems to have a hexagonal crystal structures and can clarify the qualities that are intermediary between α-$Fe_2O_3$ and γ-$Fe_2O_3$ because it has a unique phase with a substantial room-temperature coercivity, coupled magnetoelectric properties, and significant ferromagnetic resonance [11,13].

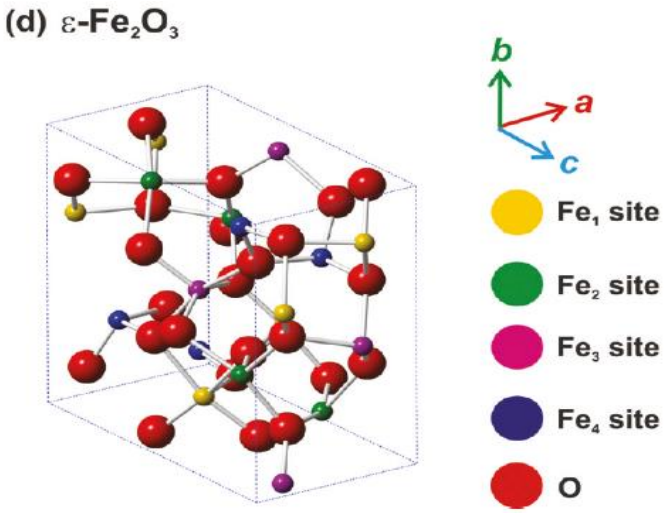


Figure 1.7 Graphical representation of ε-$Fe_2O_3$ [12].

## 1.7 Zirconium Oxide $ZrO_2$

Zirconium is a chemical compound with the symbol Zr as well as the atomic weight 40. Mineral zircon is the source of the name zirconium. It's a strong transition metal that's glossy, grey-white, and solid at room temperature. $ZrO_2$ is used in a variety of applications, including partial oxidation electrolyte, gates dielectric materials, therapeutic agents, solar panels, catalysts, and adsorbent. As a result, the production of diverse $ZrO_2$ nanostructures, such as nanotubes, nanowires, nano rods, nanoparticles and the thin films have been widely investigated in recent years [14,15].

## 1.8 Polymorph $ZrO_2$

Zirconium oxide is a polymorphous material. The three primary crystalline formations of $ZrO_2$ material are as follows [16]:

- monoclinic
- tetragonal
- cubic

### 1.8.1 Monoclinic

Baddeleyte (room temperature to 1170°C) is the mineral's most common form which has a monoclinic crystalline structure. Below 1200 °C, monoclinic $ZrO_2$ crystalline formations are thermally stable. And they're popular since they can be made at low temperatures [3].

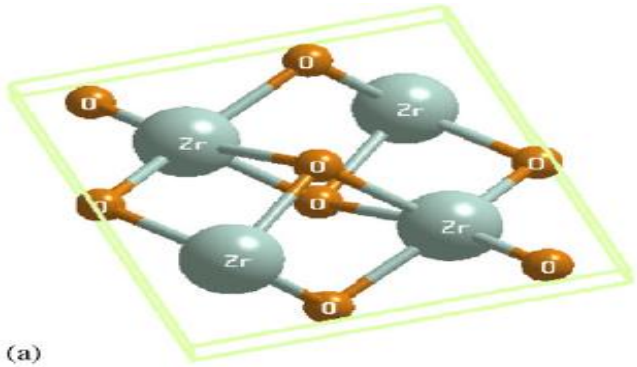


Figure 1.8 Crystal structure of monoclinic $ZrO_2$ [17].

### 1.8.2 Tetragonal

Temperatures ranging around 1200 °C to 2300 °C, tetragonal $ZrO_2$ crystalline structures are stable. It is difficult to grow its crystalline forms at temperatures below 1200 °C [3].

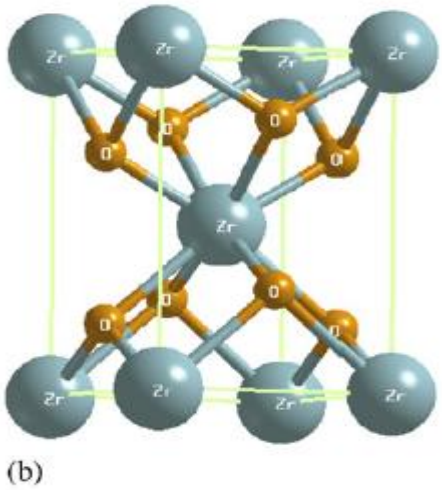


Figure1.9 Crystal structure of tetragonal $ZrO_2$ [17].

### 1.8.3 Cubic

Cubic zirconia is indeed a doped cubic crystalline zirconia that is manufactured in a wide range of shades for use as a diamond simulant and gemstone. At temperatures exceeding 2600 °C, cubic $ZrO_2$ crystalline formations are thermally stable [3].

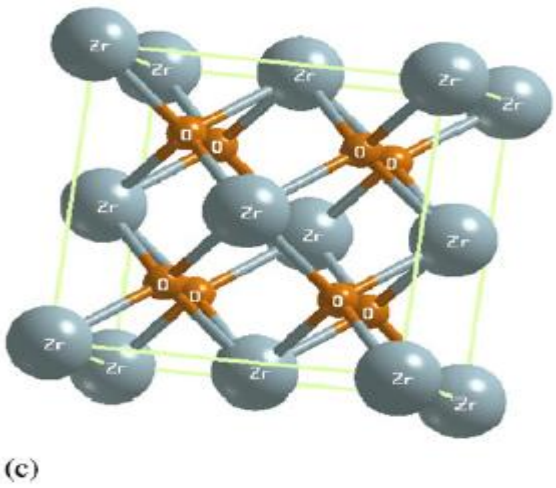


Figure 1.10 Crystal structure of cubic $ZrO_2$ [17].

## 1.9 Computational modeling

Crystallography is the discipline of study concerned with the organization and bonding of atoms found in crystalline materials, as well as the geometric structure of accessible crystalline lattice. Crystal optical characteristics are helpful in mineralogy and sciences for identifying compounds. It is important to find out the arrangement of atoms in materials to understand the relationship between properties of these materials and atomic structures [15,16].

### 1.9.1 Modeling of Crystal Structure

When developing or creating experimental settings seems to be either impossible or difficult, modelling is utilized to replace direct measurement and experimentation. Modeling theorems is indeed a scientific activity. By altering parameters, it is feasible to perform a specific aspect or the whole behavior of experimental data that is more accessible or simpler to comprehend, visualize, characterize, and reproduce. Graphical models are often utilized to visualize the various material properties [3].

## 1.10 Types of Crystals Modeling

Following six crystal systems are important for modeling atoms and molecules [18].

- Isometric or cubic
- Tetragonal
- Orthorhombic
- Monoclinic
- Triclinic
- Hexagonal

### 1.10.1 Isometric or Cubic

This system is composed of crystal containing 3 axes, which are all perpendicular to each other have identical lengths [18].

### 1.10.2 Tetragonal

This system is made up of crystal having 3 axes, that are all perpendicular to each other, just two of which are similar in length [18].

### 1.10.3 Orthorhombic

This system is made up of crystal featuring 3 mutually perpendicular axes, each of which has a distinct length [18].

### 1.10.4 Monoclinic

This system is made up of crystal bearing 3 axes that are all uneven in length. Two of the axes really aren't perpendicular to one another, however they are perpendicular to the third [18].

### 1.10.5 Triclinic

This system is made up of crystal comprising 3 axes, all of which are uneven in lengths and are therefore not perpendicular to each other [18].

### 1.10.6 Hexagonal

This system is made up of four-axed crystal. 3 of among these axes seem to be in a single plane, are properly spaced, and are of equal lengths. The 4th axes is perpendicular to all three axes [18].

## 1.11 Classification of Solids

In concern with study of structure and properties, solids are classified as:

- Crystalline Solids
- Amorphous Solids or glassy Solids
- Polymeric Solids

### 1.11.1 Crystalline Solids

Crystalline solids are ones in which the atoms and molecules are arranged in a regular pattern. Every molecule's neighbor is organized in a predictable manner that is consistent all across the crystal. The ordered structure of crystalline solids can be

studied by x-rays diffraction techniques. Some examples of crystalline solids are copper, iron, zinc, zirconia and silicon etc [19].

### 1.11.2 Motion of atoms, ions and molecules

Atoms, ions and molecules in a crystalline solid are in state of vibratory motion about fixed points. There amplitude of vibration increases with the increase in temperature. But average distance between the atomic positions remains same [19].

### 1.11.3 Amorphous or Glassy Solids

There is no predictable distribution of atoms in amorphous solids, they are much like fluids with chaotic structures froze in them. They are called solid liquids. They have no definite melting point [19].

### 1.11.4 Polymeric Solids

They are solid materials having a structure that lies somewhere between order and conflict. Polymerization relates to the procedure by which comparatively simple molecules are joined into huge long chains or three-dimensional structures via chemical processes [19].

## 1.12 X-ray Diffraction (XRD)

X-ray diffraction analysis (XRD) is a technique used in research of substances to determine material's crystalline structure. XRD involves exposing a material to arriving X-rays and thereafter evaluating the intensity as well as scattering angles of such X-rays that depart the material [20].

### 1.12.1 Powder Diffraction Patterns (XRD)

In order to define and determine the lattice parameters of a crystal structure diffraction patterns are used. Whenever the X-ray is directed at a crystal, it causes it to diffract in a pattern that is unique to the structure. In the case of powder X-ray diffraction, the diffraction peaks are derived from any material powder rather than a single crystal. Powder diffraction is simpler, more effective, and more economical

than single crystal diffraction since it does not need the creation of individual crystals [21].

### 1.12.2 Plot of Intensity

An X-ray powder diffraction pattern is indeed a plot of the intensity of X-rays that scattered at various angles using a specimen that comprises an X-ray source (typically an X-ray tube), detector, angle-changing mechanism, and sample holder. Initially, an X-ray is directed at an angle θ on the material, and the detector is set opposite to the source, reading the intensity of the X-ray it received at a angle of 2θ from the source route. The detector angle is always 2θ degrees above the source route, while the incidence angle grows with time. When the incidence X-rays strike the material in such a way that the Bragg Equation is achieved.

$$\mathrm{Sin}\theta = n\lambda/2d \qquad (1)$$

Where θ is the angle of incidence of the X-ray, n is an integer, λ is the wavelength and d is the spacing between atom layers. As a result, constructive interference as well as a peak in intensity will occur. This X-ray signal is recorded and processed by a detector, which then transforms the signal to an intensity ratio that is sent to a machine [21,22].

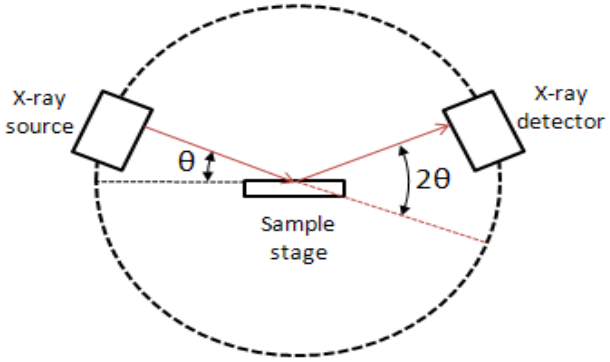


Figure 1.11 Represents the Powder X-ray Diffractometer's equipment [20].

### 1.12.3 Applications of Powder X-ray Diffraction

The most common use of X-ray powder diffraction is to identify an unknown crystalline substance. Following are some applications of powder X-ray diffraction

- crystalline material characteristics
- identifying fine-grained minerals
- calculating unit cell dimensions
- determine crystal structures [22].

## 1.13 Applications for analyzing Crystal Structures

By analyzing crystal structure on basis of x-ray crystallography will gives hundreds of applications. It was mostly employed in basic scientific applications. To determine the size of atoms, the molecular geometry of materials, the lengths and distinct types of chemical bonds, film thickness, the difference between composites at the atomic scale, crystal stability, grain alignment, and size distribution. It is presently utilized to determine the structure of a wide range of biological compounds, including vitamins, pharmaceuticals, thin-film and multi-layered materials. The most extensive application of it is to investigate precise ways in which the structure of a materials, medication, or chemical will interact in different surroundings [23].

# RATIONALE

The scope of this study is to understand, simulate and define different parameters of $ZrO_2$ and $\alpha$-$Fe_2O_3$ by 3-D visualization. The main goal is to explore different parameters in terms of crystal structures, fractional coordinates and lattice planes for metal oxides polymorphs by using VESTA software for better understanding.

# OBJECTIVES

Following are the objectives of this study:

- To visualize the 3-D structures of polymorph $ZrO_2$ and $\alpha$-$Fe_2O_3$.
- To understand strategies used for visualization of atoms, ions and molecules.
- This study visualized various aspects of $ZrO_2$ and $\alpha$-$Fe_2O_3$.

# CHAPTER 2

# LITERATURE REVIEW

I Purnamasari et al. (2021) studied sol-gel technique crystal structure of Lanthanum Orthoferrite doped Zirconium $LaFeZrO_3$ for solar cell contender. The crystal structure characteristics of $LaFeZrO_3$ powder were analyzed using X-ray diffraction. Crystal structure's geometric characteristics were determined by the VESTA software. According to the findings, the sample has an octahedral geometry with a Pnma space group. When the zirconium concentration is increased, the lattice parameters for 0.075, 0.1, and 0.15 rise according to X-ray diffraction analysis, while the crystal size of $LaFeZrO_3$ falls and displays nanosize [24].

Davinder Kumar et al. (2020) synthesized pure and nickel doped zirconium oxide $ZrO_2$ samples, namely N1, N2, N3, N4, using the sol-gel technique, at doping levels of 0, 1, 3, and 5 molar percentage distribution, sequentially. X-ray spectroscopy was used to validate the structure of the material that were discontinuous of energy. Rietveld refinement, X-ray diffraction measurements showed that the tetragonal phase was stabilized with several monoclinic phase impurities. The decrease in crystallite size resulted in an increase in unit cell volume. Because of the combined impact of quantum confinement as well as the formation of interstitial sites, UV-visible spectroscopy indicated a fluctuation in optical band gap with increasing Ni dopant in $ZrO_2$ nanocrystals [25].

Amita et al. (2020) illustrated the α-phase of $Fe_2O_3$ Patterson densities in terms of model electron densities and model nuclear densities. The crystallographic display of Patterson densities of α-$Fe_2O_3$ is accomplished out theoretically using VESTA software. The investigated result is primarily because of packing ratio of α-$Fe_2O_3$ and suggests that α-$Fe_2O_3$ could be used as an ultraviolet blocking agent in paints [26].

Laura Madalina Cursaru et al. (2020) studied the influence of temperature and pressure here on structural and magnetic properties of iron oxide nanoparticles formed by hydrothermal synthesis, that are manufactured at temperature between 100–200$^{o}$ C and pressures of 20–1000 bar. The crystalline phase iron oxide is influenced by pressure. The results of Mössbauer characterization demonstrate that hematite forms at low pressure while goethite forms at high pressure. The results of the thermal study match those of the X-ray diffraction particle size analysis, indicating that the produced iron oxides have crystallized [27].

M. Ounacer et al. (2020) studied structural and magnetic properties of iron oxide nanoparticles The sample was created through co-precipitation and annealed at various temperatures. The annealed samples were studied using X-ray diffraction, scanning electron microscopy, transmission electron microscopy, vibrating sample magnetometry, and Mössbauer spectroscopy. The X-ray diffraction results show the formation of three components: magnetite $Fe_3O_4$, maghemite γ- $Fe_2O_3$, and hematite $\alpha$-$Fe_2O_3$. Magnetite and maghemite had crystallite sizes that were equivalent, whereas hematite had bigger crystalline structure [28].

Anamika Ghosh et al. (2020) synthesized six chemical ways to study iron oxide's structure and magnetic characteristics. Although all synthesis processes produce particles in the nanoscale range, the average crystallite size distribution differ depending on the technique. Current investigations of room temperature and low temperature magnetic data support the occurrence of superparamagnetic form in 6-8 nm particles. Graphically depicted Rietveld refining of XRD patterns for samples generated using six different chemical processes [29].

Naveen Kumar et al. (2019) illustrated different crystallinity, fractional coordinates and lattice planes of transition metal polymorphs with almost the identical arrangement but distinct crystal structures, particularly $ZrO_2$. Using the VESTA programme, it was possible to view the crystallographic depiction $ZrO_2$ along with the computing bond length between Zirconium and Oxygen. The length of the bond is measured in Angstrom [3].

R. M. Kershi et al. (2018) analyzed the effect of rare metal ions substitutions on the morphological, translational, optic, electrical, and magnetic properties of super - paramagnetic iron oxide and (RE = Dy, Nd, La) nanoparticles synthesized using the co-precipitation technique. X-ray diffraction, scanning electron microscopy, UV–Vis spectroscopy, vibrating sample magnetometer, two-probe method, and LCR bridge were used to characterize the materials. The characteristic phase of magnetite structure is revealed by X-ray diffraction patterns of all samples, The $NdFe_3O_4$ sample contains a trace of ortho-ferrite as a secondary phase. Saturation magnetization in the samples spans from 41.8 to 52.3 emu/g and reduces with RE ion doping as the ionic radius rises. As the ionic radii of dopants rise, the samples' dielectric constant drops as their activation energy rises [30].

Piyush Siroha et al. (2018) studied highly ordered transition metal oxide nanostructures, particularly $Fe_2O_3$ and $TiO_2$, have been studied experimentally and theoretically. The crystallographic representation of polymorphs $Fe_2O_3$ ($\alpha$ -$Fe_2O_3$) and $TiO_2$, this work demonstrates the use of VESTA software can create anatase, brookite and rutile-$TiO_2$, nanomaterials. Representation of different categories on the basis of crystalline structure and lattice plane for transition metal oxide nanocomposites, specifically $Fe_2O_3$ and $TiO_2$ were produced. The computed bond-length of iron Fe and titanium Ti materials with oxygen O, as well as the bond length of iron Fe and titanium Ti materials with oxygen O, was calculated in angstroms [11].

J.A. Sans et al. (2018) studied the nature and stability of ε- $Fe_2O_3$ volume collapse at severe circumstances. It necessitates a thorough examination of the evolution of polyhedral units under compression. Rietveld refinements were used to create the structures. The results show that this material, which has exceptional magnetic characteristics, can withstand pressures of up to 27GPa. Above 27GPa, volume collapse occurs, causing tetrahedrally coordinated iron to shift to an octahedral state [31].

Yi-Feng Lin et al. (2015) synthesized that by using a hydrothermal technique monoclinic $ZrO_2$ nanoparticles were created. When phenol was mixed to the

resulting solution for the hydrothermal process, ZrO2/phenol formaldehyde (PF) polymers featuring tetragonal ZrO2 crystalline forms were generated. Tetragonal ZrO2 phases form well in higher PH values and OH- concentration solutions. Production of PF aids the transition to tetragonal $ZrO_2$ from monoclinic $ZrO_2$. Following techniques were used X-ray diffraction patterns, scanning electron microscopes and tunneling electron microscopes [14].

Keith P. McKenna et al. (2014) studied the three-dimensional geometry that was a blend of predicted 1st principle modelling as well as high-resolution transmission electron microscopy, was used to clearly pinpoint the location of the universal antiphase barrier in magnetite. The atomic scale morphology and structure of very persistent antiphase threshold defects in $Fe_3O_4$ were visualized using VESTA software. These [110] planar boundary flaws are remarkably persistent, resulting in antiferromagnetic interaction amongst neighboring domains, explaining the magnetoresistance and reduced spin polarization that are frequently reported [32].

Yoshiro Ohgi et al. (2011) evaluated that at 1000$^oC$ partially oxidized zirconium carbonitrides Zr-CNO were used as a quasi metallic cathode in polymer electrolyte fuel cells with oxygen partial variation influences from $10^{-2}$ to $10^{-18}$ atm. Highly active Zr-CNOs have lower lattice parameters, which could be due to the production of oxygen and zirconium vacancies in monoclinic $ZrO_2$. When some amount of carbon in highly active Zr-CNOs was reduced during partial oxidation processes, the oxygen concentration on the surface was considerably reduced. This suggests that the carbon deposited in the soil operated as a powerful reduction agent. According to XPS and XRD investigations, there's also a linear relationship in between current and the quantity of oxygen vacancy formed in monoclinic structure [33].

Libor Machala et al. (2011) studied nanometric Iron(III) Oxide undergoes polymorphous changes. To prepare a particular $Fe_2O_3$polymorph as a single phase, it is critical to regulate the factors that produce polymorphous transitions. The framework and kinetics of polymorphous $Fe_2O_3$ transitions for a pure material properties like crystalline configuration, grain size, morphology, protective

coatings, aggregate stability, particle inclusion inside a lattice, external parameters of synthetic and natural conditions like temperature, pressure, atmosphere were studied and analyzed using atomic force microscopy, Mossbauer spectroscopy and tunneling electron microscope [12].

Jian Ding et al. (2011) investigated the innovative amorphous iron oxide created using a wood framework has structural and optical features. Using Fourier transform infrared and Raman spectroscopy, the porous iron oxide produced was identified as α- $Fe_2O_3$. Bond length of Fe–$O_1$ in permeable iron oxide is very close to that published for the α- $Fe_2O_3$ crystal structure, however the bond lengths of Fe–$O_2$ and Fe–Fe fluctuate from all of those found for the α- $Fe_2O_3$ crystal structure [34].

Guoliang Zhen et al. (2011) studied a new method for making cubic and spherical superparamagnetic iron oxide nanoparticles. Cubic nanoparticles having width of 8nm can be created that are very monodisperse. Using X-ray powder diffraction, high resolution transmission electron microscopy analysis, superconducting quantum interference device measurements and relativity measurements performed in a magnetic resonance imaging scanner, a detailed study of the physical properties of these nanoparticles is presented. Cubic iron oxide nanoparticles were investigated for having four times degree of crystallinity and relativity as their spherical counterparts [35].

# CHAPTER 3

# METHODOLOGY

## 3.1 VESTA

### 3.1.1 Introduction

VESTA is a 3D visualization software or application for structural models, crystal morphologies, including volumetric data like electron and nuclear densities. VESTA software simulates structures that are more precise and have immediate responsiveness. VESTA software is a viable option because it is portable and publicly available. It is simple to use and may create stunning crystal structures. Dr. Ruben A. Dilanian and Dr. Fujio Izumi created VESTA. Visualization is a method of creating visuals, graphs, and movements. Because of advances in contemporary structure refinement procedures, it is now easier and more practical to calculate three-dimensional distributions of electron densities via X-ray diffraction patterns. These technological advancements raise the requirement for integrated 3-D visualization system. It deals including both structural model and volumetric data [3,36].

## 3.2 Features of VESTA

Following are the features of VESTA

- Work in the same window with numerous structural models, volumetric data, and crystal morphologies.
- Support for numerous file-related tabs
- Project Integration for numerous file-related tabs
- Use RIETAN-FP to see constrained interatomic lengths and bond angles in Rietveld analysis.
- Transparent iso-surfaces may be layered on top of structural models.

According to the results of the analysis, we can readily view, comprehend, and characterize the crystallography representation of such oxide-based nanomaterials that seem to be appropriate for numerous energy, environmental, and security applications by utilizing this program [11,36].

## 3.3 Explanation

### 3.3.1 Window based platform

The program VESTA runs on Windows, Mac OS X, and Linux.

### 3.3.2 Innovative approaches for drafting boundary specifications

Polyhedral coordination and molecules aren't really truncated. Designing parameters for model specification can be changed in a variety of ways, similar to combining and recursive convoluting fields. Cutoff planes, in contrast to x, y, and z ranges, is being used to define drawing borders [36].

### 3.3.3 Exhibit Crystallographic details

VESTA provides diversity in crystallographic information by selecting objects like atoms, bonds, and coordination polyhedral using a mouse. Following are some crystallographic information provided by VESTA:

- Display fractional coordinates.
- It provides site symmetry, Wyckoff letters and site multiplicities.
- Provides information about concerning primary axes and the mean square displacements for displaying anisotropic thermal motion.
- Displays interatomic distances, torsion angles and bond angles [36].

### 3.3.4 Lattice Modification

VESTA has a function that allows it to transform generalized corresponding position in a standard context into those in a non-conventional context by employing a transformation matrix, that is also used for primitive lattice into complicated lattice transformations and edifice building. On top of a structural framework, translucent iso-surfaces could be overlaid [36].

## 3.4 Dealing with volumetric data

### 3.4.1 Visualization

Iso-surfaces are represented by smooth-shaded polygons, wireframes, and dot surfaces. Technological parameters including both positive and negative points, such as wave functions and nuclear concentrations, can be visualized as iso-surfaces with two distinct hues [36].

### 3.4.2 Multiple 3D data pixel operations

VESTA makes it possible to perform pixel computations on much more than two 3D data sources, and each set of data could be increased by any value. This property, for instance, enables us to differentiate predicted electron densities from observed ones obtained by MEM analysis in designed to detect luminous particles lacking in a structural model and to differentiate down spin electron densities from up spin ones in order to display functional spin density [36].

### 3.4.3 Coloring surfaces

VESTA includes an appealing capability for coloring iso-surfaces, which is commonly used to coloring iso-surfaces of electron densities based on electrostatic potential [36].

### 3.4.4 Exhibit lattice planes

It is possible to add crystal planes of varying opaqueness. Throughout 3D pixel data, data points are used to color boundary sections and lattice planes respectively. You may use the Comment Section to list peak values and locations in 3D pixel data [36].

**Mechanism to calculate fractional coordinates, lattice planes, structural models and powder diffraction patterns (XRD) by using VESTA software is given in this flowchart and details will be discussed in further sections.**

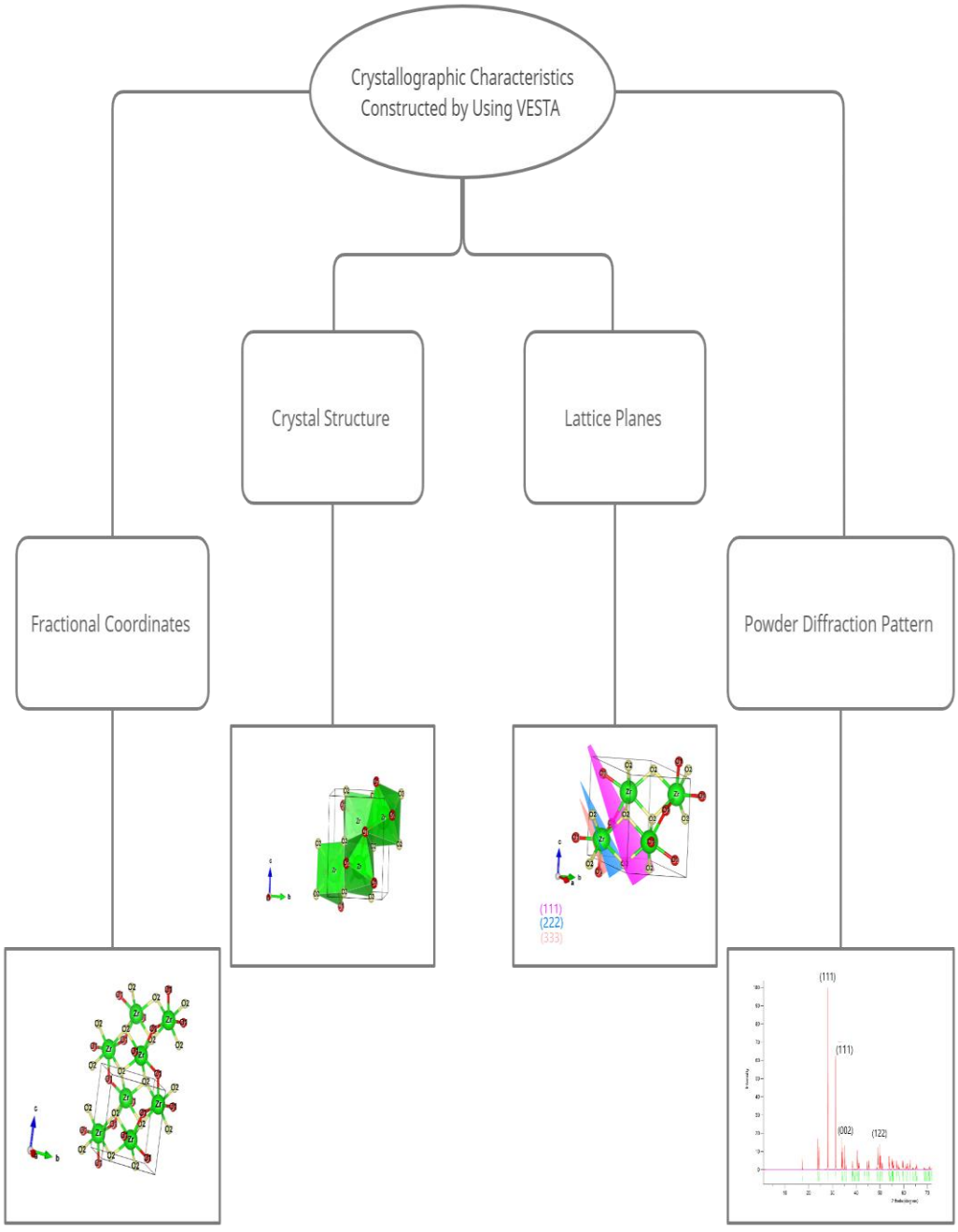

## 3.5 Construction of Structure of $ZrO_2$

### 3.5.1 Main Window

The first step is to open a page at VESTA is known as Main Window as shown in Figure 3.1.

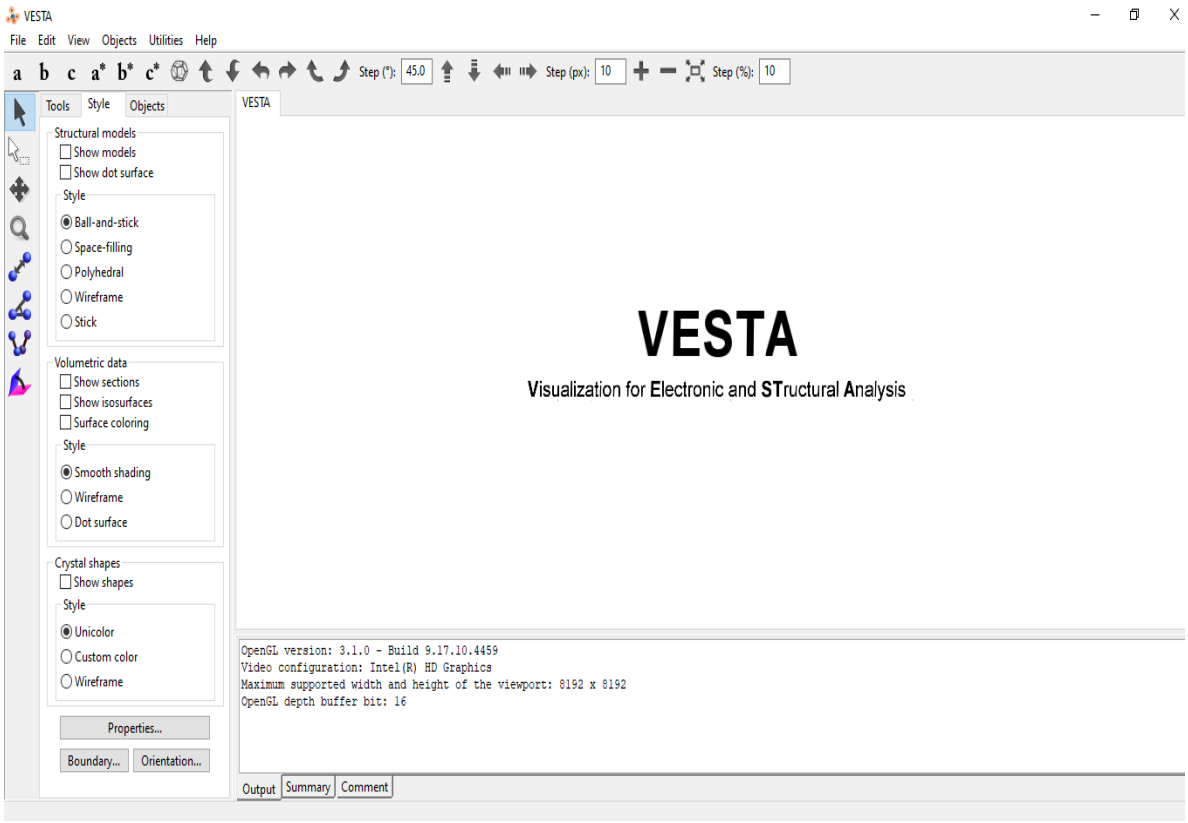


Figure 3.1 Main Window of VESTA [36].

### 3.5.2 Unit Cell

Next step in order to construct a crystal structure of $ZrO_2$ click on 'edit' from top bar of main window and then click on 'unit cell' from the menu bar as shown in Figure 3.2.

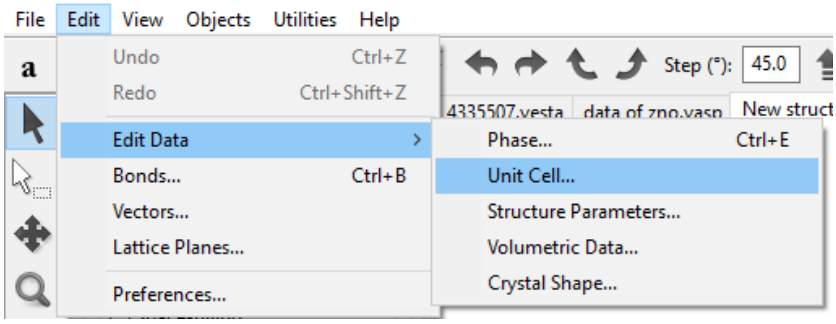


Figure 3.2 Selecting unit cell for construction of crystal structure [36].

.

### 3.5.3 Selecting Parameter

Selecting parameters for monoclinic Zirconium oxide $ZrO_2$ in 3-dimensions for making a monoclinic crystal structure. After clicking on 'unit cell', in next step another window will appear where we can select their symmetry and lattice parameters for construction of $ZrO_2$ as shown in Figure 3.3. Type of lattice selected for this is 'R' and space group number 14 P 21/c. Then click on 'Apply' and 'Ok' to execute.

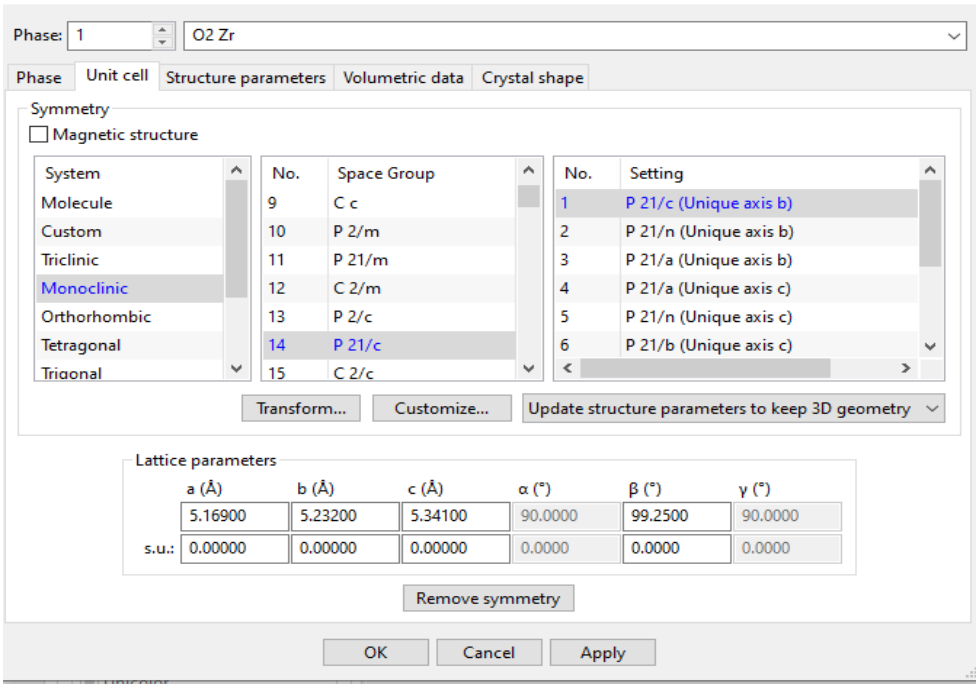


Figure 3.3 Selecting symmetry of unit of cell $ZrO_2$ [36].

## 3.6 Construction of Structure of $\alpha$-$Fe_2O_3$

### 3.6.1 Main Window

The first step is to open a page at VESTA is known as Main Window as shown in Figure 3.1.

### 3.6.2 Unit Cell

In order to construct a crystal structure of $\alpha$-$Fe_2O_3$, click on 'edit' from top bar of main window and click on 'unit cell' from bar menu as shown in Figure 3.2.

### 3.6.3 Structure parameters

Structure parameters of Iron Fe and Oxygen O are selected in 3-dimensions for making a rhombohedral crystal structure. Type of lattice selected for this is 'R' and space group number 167 R -3 c. After clicking on 'unit cell', in next step another window will appear where we can select their symmetry and lattice parameters for construction of $\alpha$-$Fe_2O_3$ as shown in Figure 3.4. Then click on 'Apply' and 'Ok' to execute.

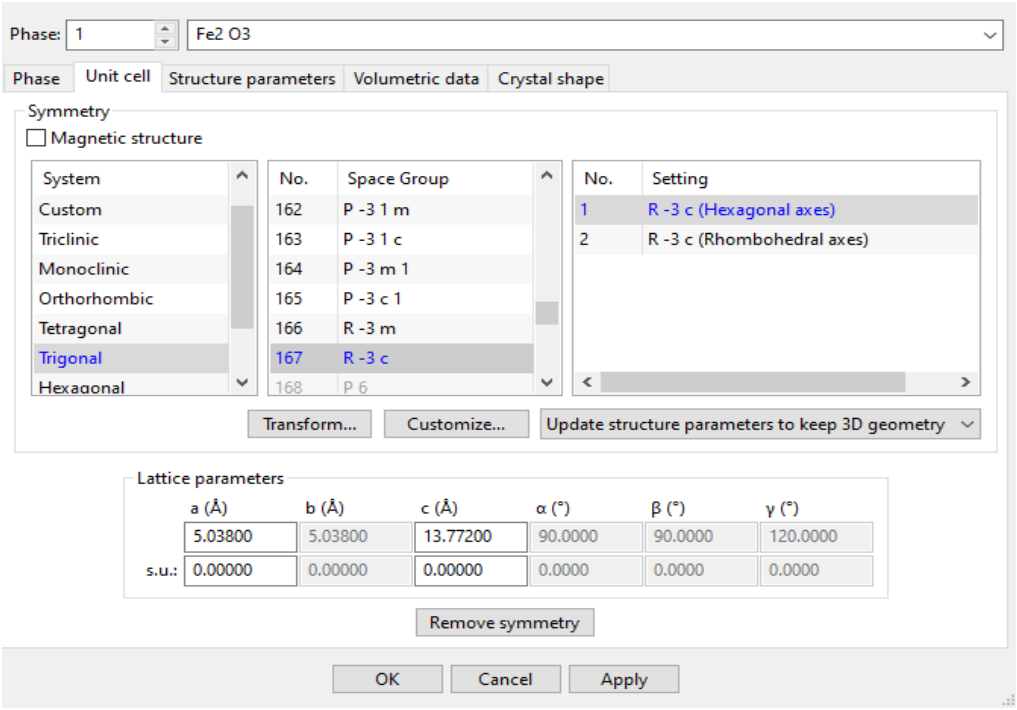


Figure 3.4 Selecting symmetry of unit cell for $\alpha$-$Fe_2O_3$ [36].

## 3.7 Crystal Structure Models in VESTA

VESTA software display crystal structures in following five different models for both $ZrO_2$ and $\alpha$-$Fe_2O_3$ by clicking on following structural models as shown in Figure 3.5.

- Ball and stick
- Wireframe
- Space filling
- Polyhedral
- Stick models

### 3.7.1 Ball and Stick

In this structures are constructed by connecting atoms with each other with the help of a stick between them. And makes a style of ball and stick.

### 3.7.2 Wireframe

In this structures are constructed by connecting atoms in wireform. And makes a style of wireframe.

### 3.7.3 Space Filling

In this structures are constructed by filling space between atoms by increasing their size and atomic size of some atoms are greater than others. And makes style of space filling.

### 3.7.4 Polyhedral

In this structures are constructed by connecting atoms involving in a polyhedral form. And makes a style of polyhedral.

### 3.7.5 Stick

In this structures are constructed by using a stick model as bond between different atoms. And makes a style of stick.

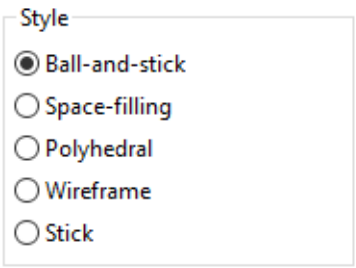


Figure 3.5 Structural Models from VESTA [36].

## 3.8 Lattice Planes

### 3.8.1 Inter-planar Distances

In order to insert lattice planes first step is to calculate inter planar distance between three adjacent values of miller indices (h k l) for both $ZrO_2$ and $\alpha$-$Fe_2O_3$. The spacing d between adjacent (h k l ) lattice planes in monoclinic crystals of $ZrO_2$ with lattice constant a is calculated by using formula

$$d_{hkl} = \frac{a}{\sqrt{h^2+k^2+L^2}} \qquad (1)$$

While on the other hand spacing d between adjacent (hkl) lattice planes in rhombohedral crystals with lattice constants a and c is calculated for $\alpha$-$Fe_2O_3$ by using formula

$$d_{hkl} = \frac{a}{\sqrt{\frac{4}{3}(h^2+k^2+hk)+\frac{a^2}{c^2}L^2}} \qquad (2)$$

### 3.8.2 Zirconium oxide $ZrO_2$

For inserting lattice planes in unit cell of $ZrO_2$ click on ‘edit’ from the top bar and select ‘lattice planes’ from the pop-up menu bar as shown in Figure 3.6.

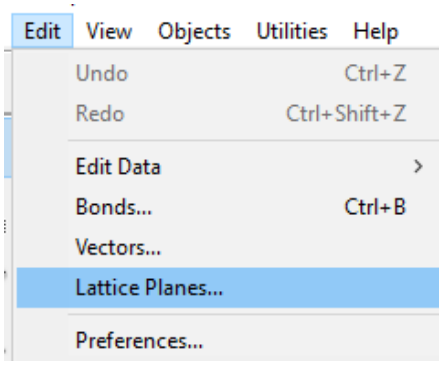


Figure 3.6 Selecting lattice planes [36].

After selecting ‘lattice planes’ a small window will appear where we can fill the values accordingly for each lattice plane with inter planar distance d as shown in Figure 3.7.

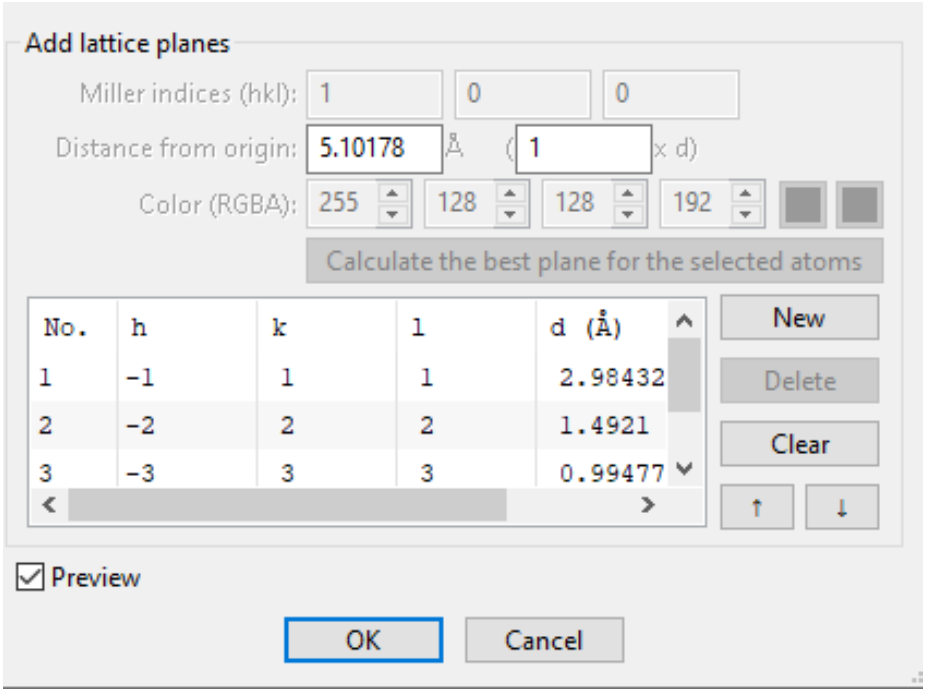


Figure 3.7 Inserting lattice planes in crystal structures [36].

### 3.8.3 Iron Oxide $\alpha$-$Fe_2O_3$

For inserting lattice planes in unit cell of $\alpha$-$Fe_2O_3$ click on ‘edit’ from the top bar and select ‘lattice planes’ from the pop-up menu bar as shown in Figure 3.6. After selecting ‘lattice planes’ a small window will appear where we can fill the values

accordingly for each lattice plane with inter planar distance d as shown in Figure 3.7.

## 3.9 Range of Fractional Coordinates

### 3.9.1 In case of $ZrO_2$

Ranges of fractional coordinates of zirconium oxide can be determined by clicking on icon ‘Boundary’ present at left most bottom corner of main window as shown is Figure 3.8.

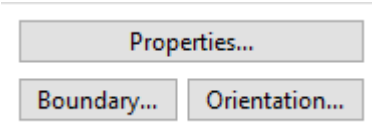


Figure 3.8 Selecting boundary from VESTA [36].

A small window will appear where we can edit the ranges of fractional coordinates as shown in Figure 3.8. And fill the values accordingly.

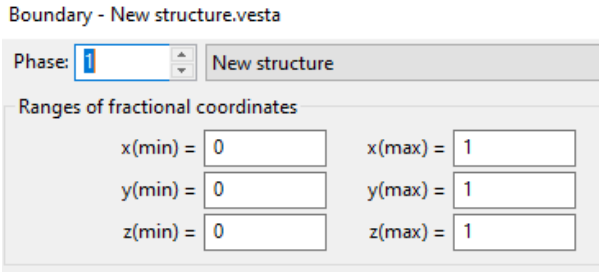


Figure 3.9 Inserting ranges of Fractional coordinates [36].

### 3.9.2 In case of $\alpha$-$Fe_2O_3$

Ranges of fractional coordinates of Iron oxide $\alpha$-$Fe_2O_3$ can be determined by clicking on icon ‘Boundary’ present at left most bottom corner of main window as shown in Figure 3.8. A small window will appear where we can edit the ranges of fractional coordinates as shown in Figure 3.9.

## 3.10 Powder Diffraction Patterns

In order to find powder diffraction pattern for Zirconium oxide $ZrO_2$ and Iron oxide $\alpha$-$Fe_2O_3$ click on 'Utilities' from the top bar in main window. A menu will appear where we select "powder diffraction patterns' that will gives the graphical representation of that particular crystal structure diffraction patterns as shown in Figure 3.10. And then click on 'calculate' This process will be repeated for both Zirconium oxide $ZrO_2$ and Iron oxide $\alpha$-$Fe_2O_3$ in order to find their diffraction patterns.

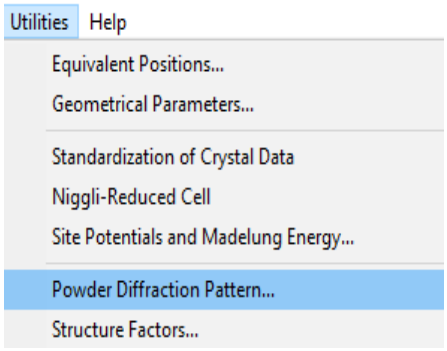


Figure 3.10 Powder Diffraction Pattern from VESTA [36].

# CHAPTER 4

# RESULTS AND DISCUSSION

## 4.1 Crystallographic Models for $ZrO_2$

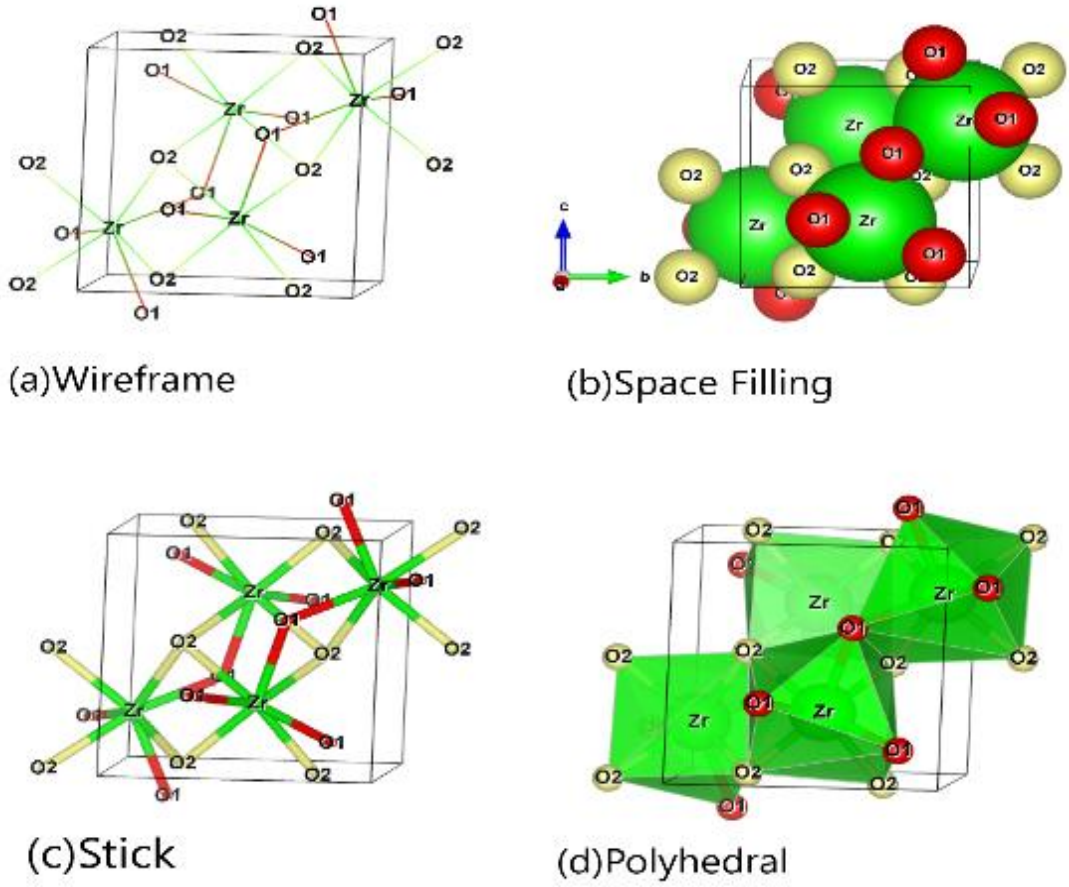


Figure 4.1 shows crystallographic models. (a) Wireframe, (b) Space Filling, (c) Stick, (d) Polyhedral for $ZrO_2$.

In term of crystallographic representation models of monoclinic $ZrO_2$ polymorphs are shown in Figure 4.2. Color Code is Red and yellow (small) sticks and sphere represents Oxygen (O) atoms while Green (large) sticks and sphere represents Zirconium (Zr) atoms. Figure 4.1 shows structural characteristics of Zirconium oxide $ZrO_2$. (a-d) Figures shows crystal structure modeling of monoclinic $ZrO_2$.

Figure 4.1 (a) shows a wireframe structure that represents the structure in wire form and there are no balls and sticks. Figure 4.1 (b) shows a space filing structure that represents atomic size of zirconium (Zr) is bigger than oxygen (O). Figure 4.1 (c) shows a stick model that represents only stick as bond between Zr and O. Figure 4.1 (d) represents polyhedral structure of monoclinic polymorph $ZrO_2$. Atoms of Zr and O are present in different colors in order to distinguish from each other. This makes by visualization of atoms ions and molecules possible to understand and estimate various aspects of crystal structure. And calculated values are in good agreement with by previously reported values.

## 4.2 Crystallographic Models for $\alpha$-$Fe_2O_3$

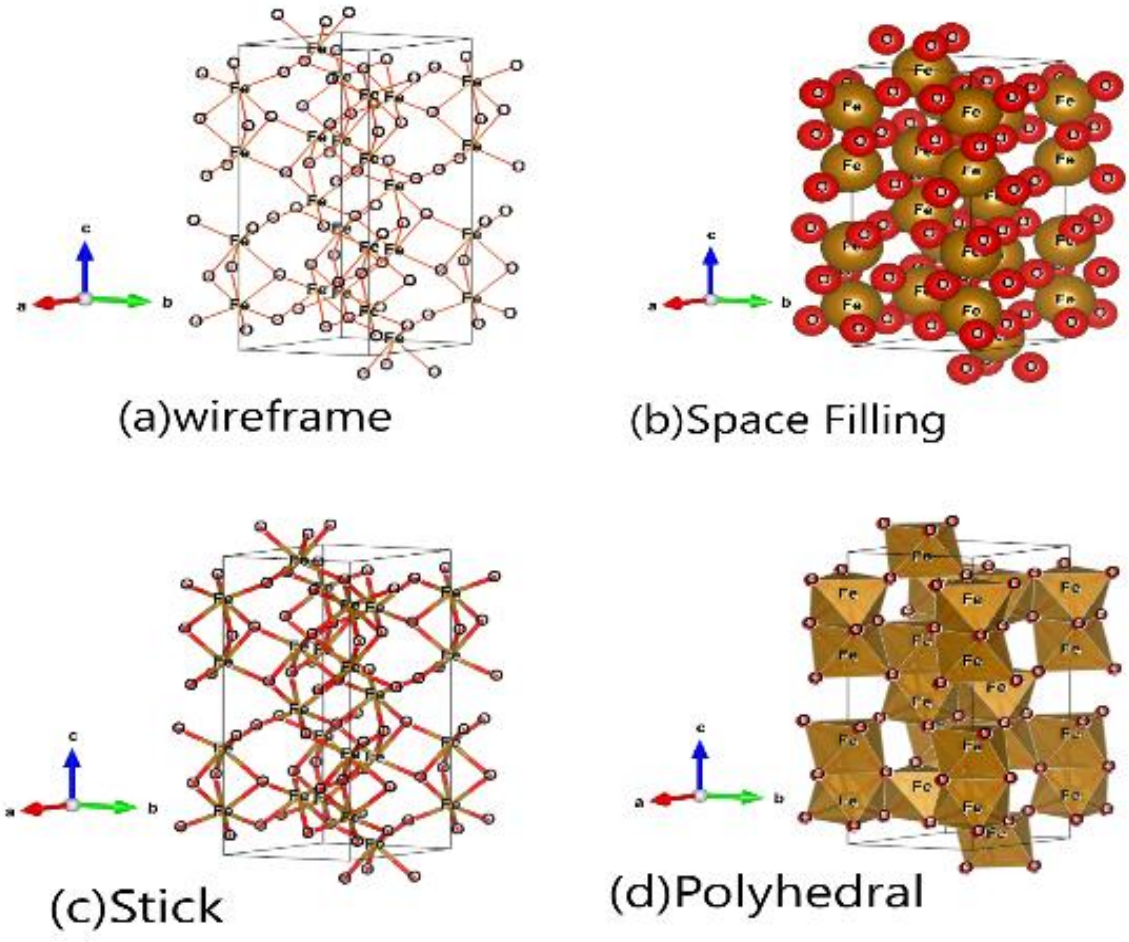


Figure 4.2 shows crystallographic models. (a) Wireframe, (b) Space Filling, (c) Stick, (d) Polyhedral for $\alpha$-$Fe_2O_3$.

In Figure 4.2 models of rhombohedral $\alpha$-$Fe_2O_3$ polymorphs are shown in terms of crystallographic representation. Color Code is Red (small) sticks and sphere represents Oxygen (O) atoms while Mustard (large) sticks and sphere represents Iron (Fe) atoms.

Figure 4.2 shows structural characteristics of iron oxide $\alpha$-$Fe_2O_3$. (a-d) Figures shows crystal structure modeling of rhombohedral $\alpha$-$Fe_2O_3$. Figure 4.2 (a) shows a wireframe structure that represents the structure in wire form and there are no balls and sticks. Figure 4.2 (b) shows a space filing structure that represents atomic size of Iron (Fe) is bigger than oxygen (O). Figure 4.2 (c) shows a stick model that represents only stick as bond between Fe and O. Figure 4.2 (d) represents polyhedral structure of rhombohedral polymorph $\alpha$-$Fe_2O_3$. Atoms of Fe and O are present in different colors in order to distinguish from each other. This makes visualization of atoms ions and molecules possible to understand and estimate various aspects of crystal structure. This shows that calculated values are close approximately to previously reported values for $\alpha$-$Fe_2O_3$.

## 4.3 Ranges of Fractional Coordinates for $ZrO_2$

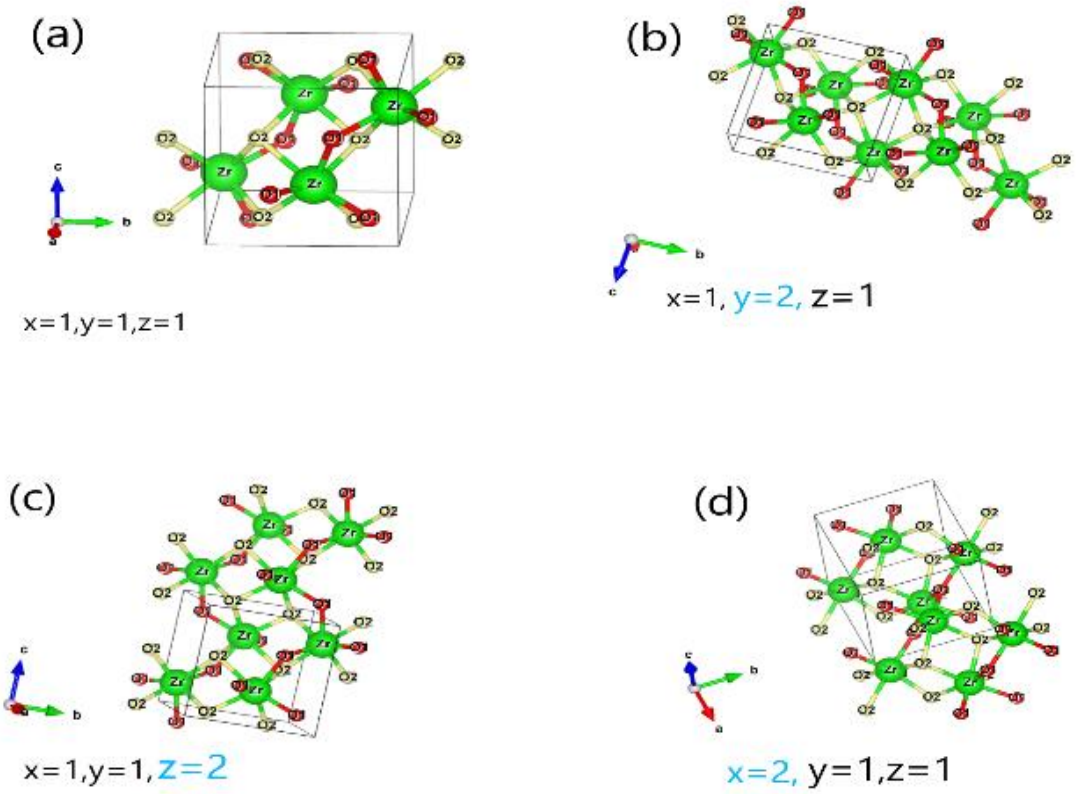


Figure 4.3 shows ranges of fractional coordinates. (a) x=1, y=1, z=1, (b) x=1, y=2, z=1, (c) x=1, y=1, z=2, (d) x=2, y=1, z=1 for $ZrO_2$.

In Figure 4.3 crystallographic representation in terms of ranges of fractional coordinates are shown for $ZrO_2$. Color Code is Red and yellow (small) sticks and sphere represents Oxygen (O) atoms while Green (large) sticks and sphere represents Zirconium (Zr) atoms.

Figure 4.3 shows crystallography in terms of ranges of fractional coordinates of polymorphs of $ZrO_2$ from (a-d). The fundamental translational vectors that are a b and c having crystallographic axis x y and z sequentially are indicated in Å. Figure 4.3 (a) illustrates ball and stick model for monoclinic polymorph $ZrO_2$ that have x=1, y=1, z=1 representing that there is only one unit cell of $ZrO_2$ and there is no transition along any axis. Figure 4.3 (b) represents range of fractional coordinates x=1, y=2, z=1 that shows one additional unit cell is along y-axis and transition of atoms was

also along y-axis. Figure 4.3 (c) illustrates x=1, y=1, z=2 that portray one additional unit cell along z-axis and transition of atoms was along z-axis. Figure 4.3 (d) shows x=2, y=1, z=1 that portray one additional unit cell along x-axis. For this previously recorded values are in good agreement with calculated values.

## 4.4 Ranges of Fractional Coordinates for $\alpha$-$Fe_2O_3$

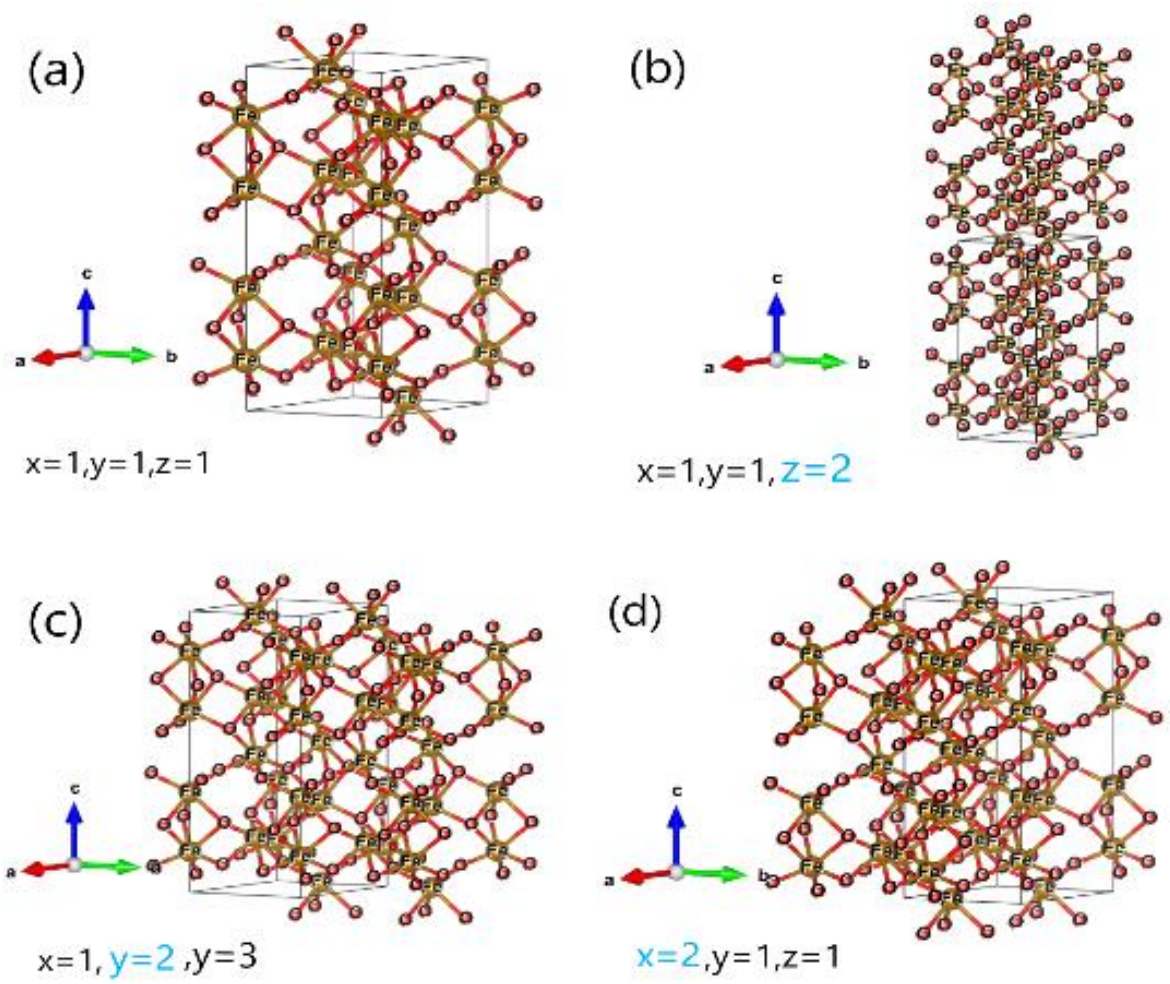


Figure 4.4 shows ranges of fractional coordinates. (a) x=1, y=1, z=1, (b) x=1, y=1, z=2, (c) x=1, y=2, z=1, (d) x=2, y=1, z=1 for $\alpha$-$Fe_2O_3$.

In Figure 4.4 crystallographic representation in terms of ranges of fractional coordinates are shown for $\alpha$-$Fe_2O_3$. Color Code is Red (small) sticks and sphere represents Oxygen (O) atoms while Mustard (large) sticks and sphere represents Iron (Fe) atoms.

Figure 4.4 shows crystallography in terms of ranges of fractional coordinates of polymorphs of $\alpha$-$Fe_2O_3$ from (a-d). The fundamental translational vectors that are a b and c having crystallographic axis x y and z sequentially are indicated in Å. Figure 4.4 (a) illustrates ball and stick model for rhombohedral polymorph $\alpha$-$Fe_2O_3$ that have x=1, y=1, z=1, representing that there is only one unit cell of $\alpha$-$Fe_2O_3$. Figure 4.4 (b) represents range of fractional coordinates x=1, y=1, z=2 that shows one additional unit cell is along z-axis. Figure 4.4 (c) illustrates x=1, y=2, z=1, that portray one additional unit cell along z-axis. Figure 4.4 (d) shows x=2, y=1, z=1 that portray one additional unit cell along x-axis. And calculated values are in good agreement with by previously reported values.

## 4.5 Lattice Planes for $ZrO_2$

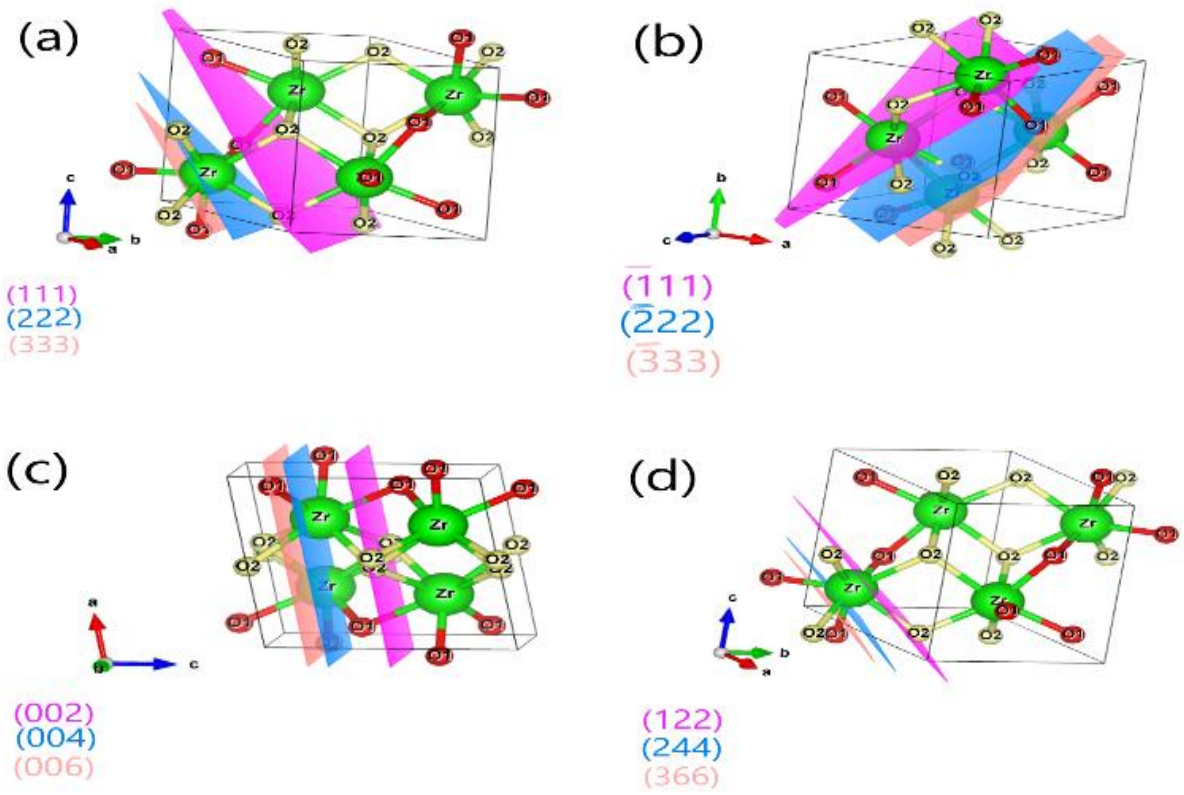


Figure 4.5 Lattice planes. (a) (111), (222), (333) planes, (b) $(\bar{1}11)$, $(\bar{2}22)$, $(\bar{3}33)$ planes, (c) (002), (004), (006) planes, (d) (122), (244), (366) planes for $ZrO_2$.

In Figure 4.5 crystallographic representation in terms of lattice planes is shown. Margenta color represents (111), $(\bar{1}11)$, (002) and (122) planes. Blue color represents (222), $(\bar{2}22)$, (004) and (244) planes. While peach color represents (333), $(\bar{3}33)$, (006) and (366) planes.

Figure 4.5 shows different miller indices (h k l) values that have different lattice planes in monoclinic $ZrO_2$ polymorphs. (a-d) Figures shows descent of lattice planes for $ZrO_2$. Figure 4.5 (a) represents lattice planes that have descent (h k l) values (111), (222), (333) planes. Figure 4.5 (b) represents lattice planes with (h k l) values $(\bar{1}11)$, $(\bar{2}22)$, $(\bar{3}33)$ planes. Figure 4.5 (c) shows lattice planes with (h k l) values (002), (004), (006) planes. Figure 4.5 (d) shows lattice planes with (h k l) values (122), (244), (366) planes. The planes are represented in different colors to distinguish planes from each other. In Zirconium oxide 3D crystal structure, lattice planes are inserted in them. Each lattice system contains a set of three miler index notation. By changing the values of axes the dimensions of lattice planes in crystal structure also changes. And the estimated values accord well with the previously reported values.

## 4.6 Lattice Planes for $\alpha$-$Fe_2O_3$

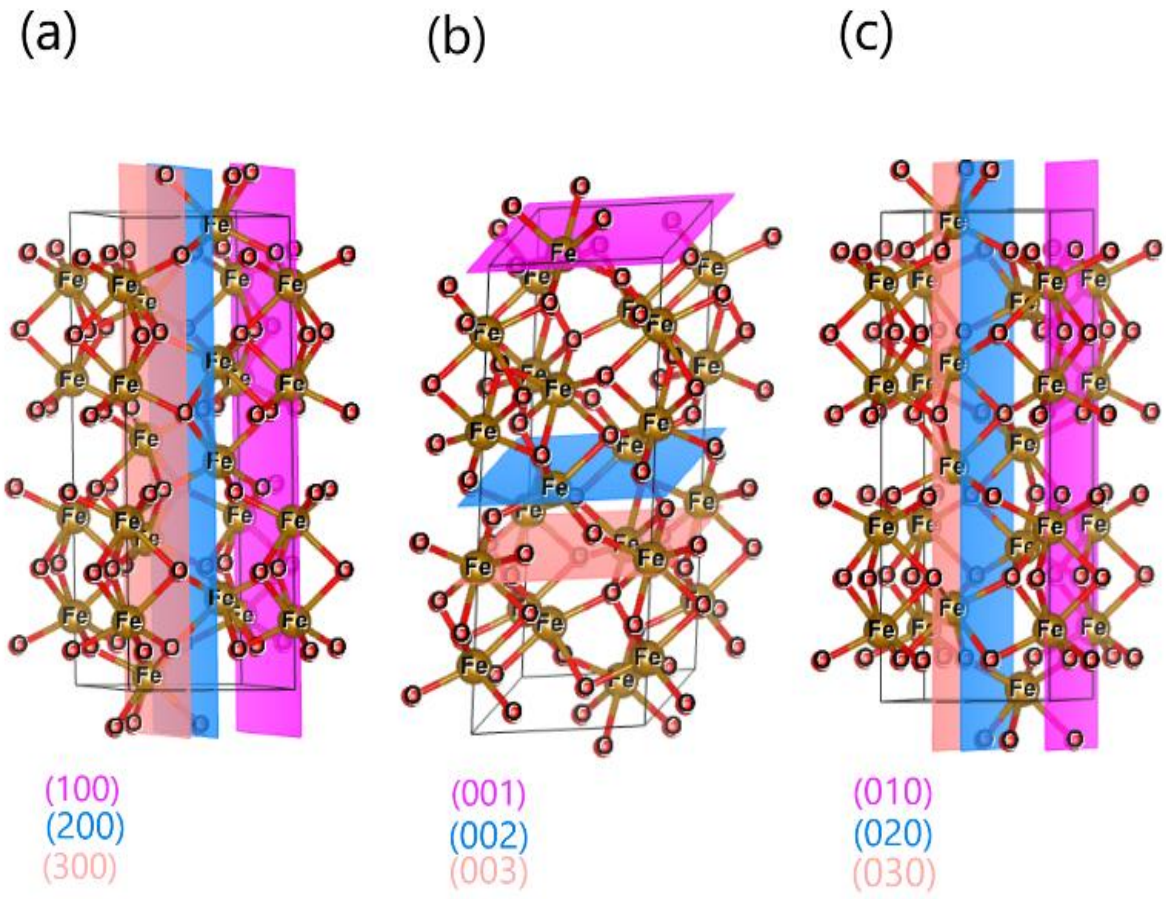


Figure 4.6 Lattice planes. (a) (100), (200), (300) planes. (b) (001), (002), (003) planes. (c) (010), (020), (030) planes for $\alpha$-$Fe_2O_3$.

In Figure 4.6 crystallographic representation in terms of lattice planes is shown. Margenta color represents (100), (001) and (010) planes. Blue color represents (200), (002) and (020) planes. While peach color represents (300), (003) and (030) planes.

Figure 4.6 shows different miller indices (h k l) values that have different lattice planes in rhombohedral $\alpha$-$Fe_2O_3$ polymorphs. (a-c) Figures shows descent of lattice planes for $\alpha$-$Fe_2O_3$. Figure 4.6 (a) represents lattice planes that have descent (h k l) values (100), (200), (300) planes. Figure 4.6 (b) represents lattice planes with (h k l)

values (001), (002), (003) planes. Figure 4.6 (c) shows lattice planes with (h k l) values (010), (020), (030) planes. The planes are represented in different colors to distinguish from each other. In Iron oxide 3D crystal structure lattice planes are inserted in them. Each lattice system contains a set of three axes. By changing the values of axes the dimensions of lattice planes in crystal structure also changes. These estimated values agree well with the previously stated figures.

## 4.7 Powder Diffraction (XRD) Pattern for $ZrO_2$

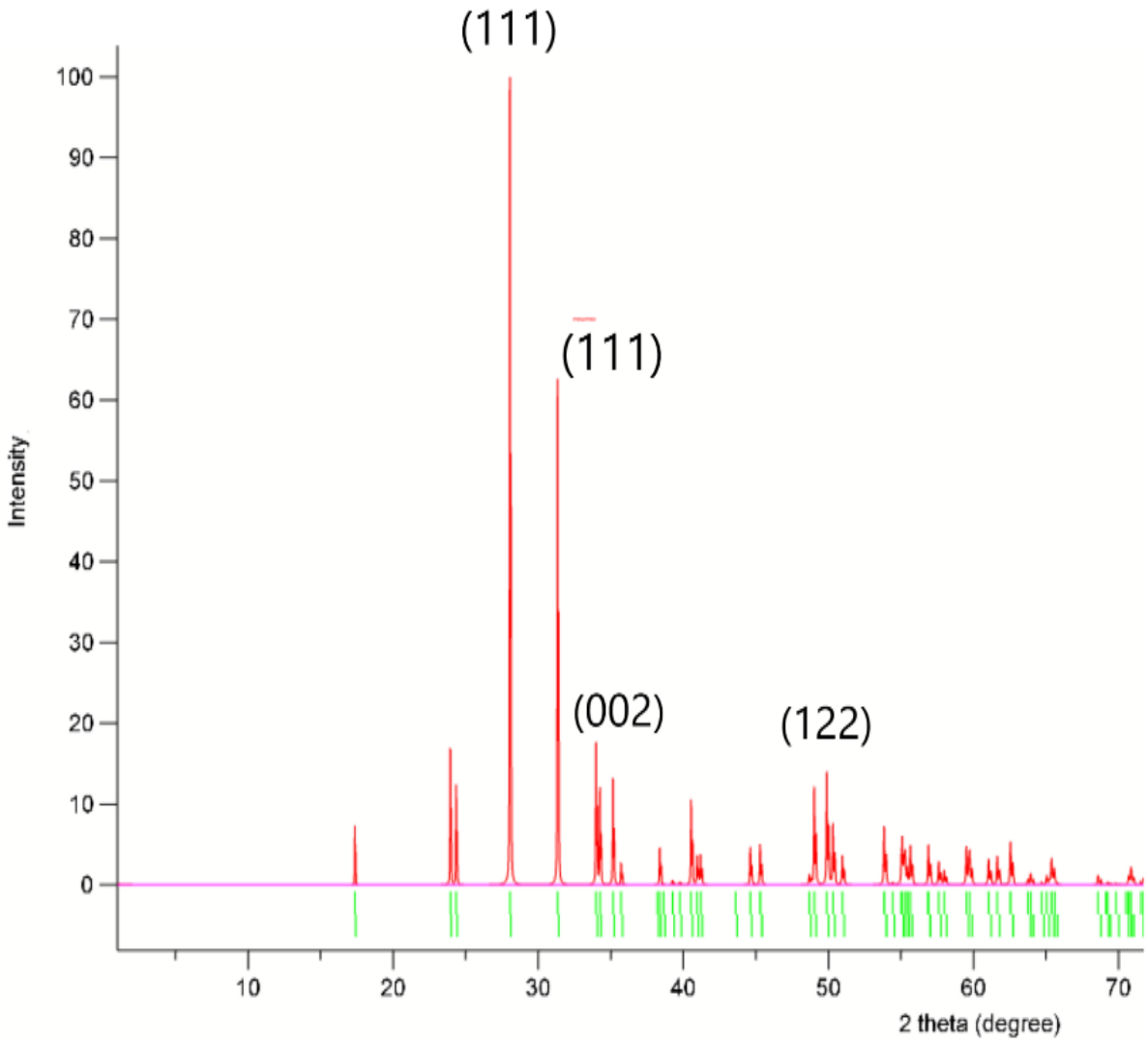


Figure 4.7 XRD pattern for $ZrO_2$ obtained from VESTA.

In Figure 4.7 most intense lattice planes of $ZrO_2$ are represented by using powder diffraction (XRD) pattern. This graph represents intensity on y-axis and angle 2Ɵ on x-axis. The highest peak appear at most intense lattice planes having (h k l) values of (111) at an angle of 28.05°. $(\bar{1}11)$ appear in powder diffraction pattern at an angle of 31.33°. (002) peak appear at angle of 34.06°. And (122) peak appear at an angle of 54.42°.

Figure 4.7 represent x-ray powder diffraction pattern (XRD) for monoclinic ZrO2polymorphs. All the observed peaks can be indexed in agreement with the expected monoclinic structure of $ZrO_2$. The peaks appearing at $2\theta$ exhibit most intense lattice planes having (h k l) values of (111), $(\bar{1}11)$, (122) and (002) planes. The $ZrO_2$ products are highly crystalline, as seen by the narrow sharp peaks. From this graph we come to known that the most dominant miller index is (111). Because when x-rays falls on the crystal sample of monoclinic $ZrO_2$ the most intense rays detected at 2Ɵ angle is (111) miller index. These estimated values agree well with the previously stated figures.

## 4.8 Powder Diffraction (XRD) Pattern for $\alpha$-$Fe_2O_3$

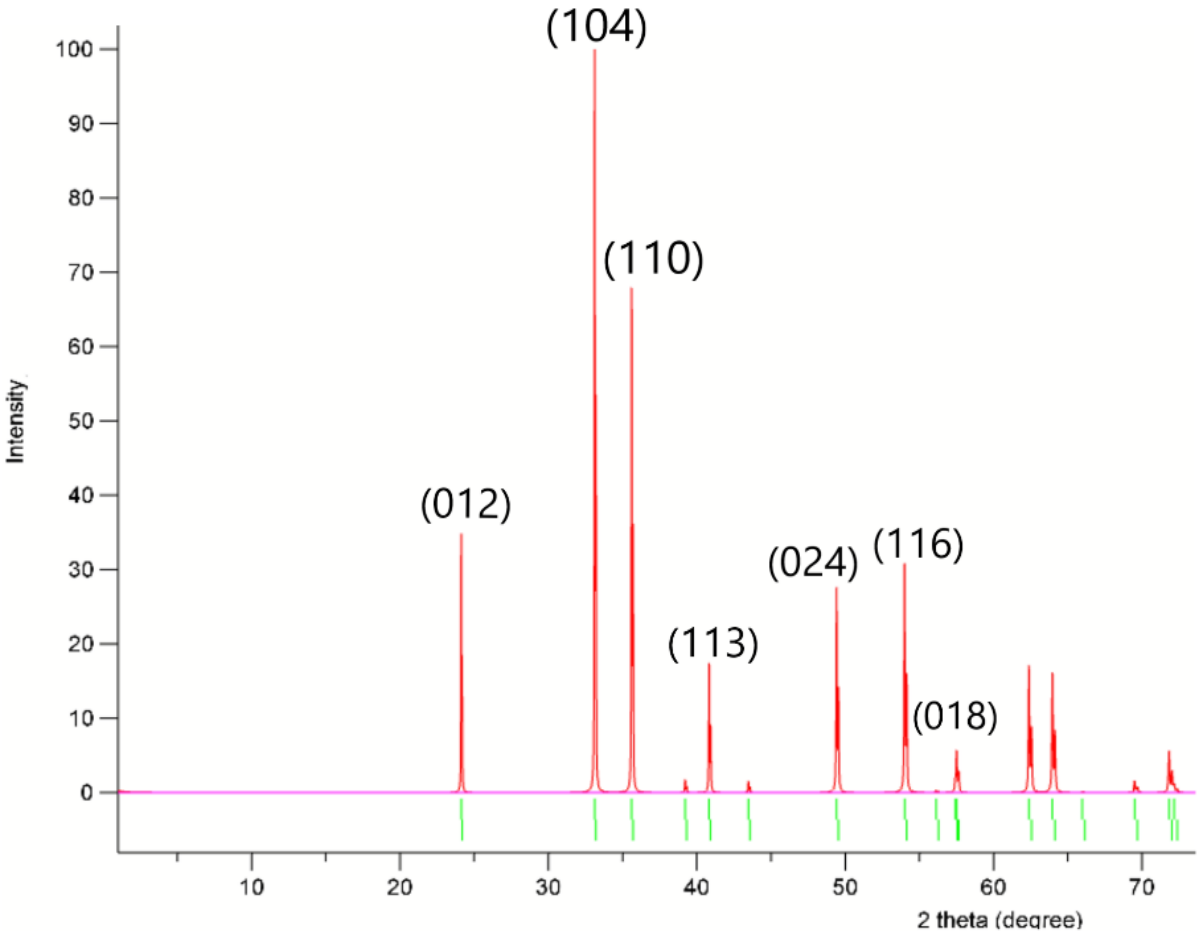


Figure 4.8 XRD pattern for $\alpha$-$Fe_2O_3$ obtained from VESTA.

In Figure 4.8 most intense lattice planes of $\alpha$-$Fe_2O_3$ are represented by using powder diffraction (XRD) pattern. This graph represents intensity on y-axis and angle 2Θ on x-axis. The peaks appearing at $2\theta$ exhibit most intense lattice planes having (h k l) values of (104) at angle of 33.11°. (012) appear in powder diffraction pattern at an angle of 24.12°. And the peaks (110), (113), (024), (116) and (018) appear at an angles of 35.61°, 40.82°, 49.54°, 54.14° and 57.65° respectively.

Figure 4.8 represents x-ray powder diffraction pattern (XRD) for rhombohedral $\alpha$-$Fe_2O_3$ polymorphs. All the observed peaks can be indexed in agreement with the expected rhombohedral structure of $\alpha$-$Fe_2O_3$. The peaks appearing at $2\theta$ exhibit

most intense lattice planes having (h k l) values of (012), (104), (110), (113), (024), (116) and (018) planes. The hematite products are highly crystalline, as seen by the narrow sharp peaks. From this graph we come to known that the most dominant miller index is (104). Because when x-rays falls on the crystal sample of rhombohedral $\alpha$-$Fe_2O_3$ the most intense rays detected at 2Ɵ angle is (104) miller index. These estimated values agree well with the previously stated figures.

Table 4.1 Illustrates lattice parameters and atomic position of Zr and O in $ZrO_2$ polymorphs.

| **Crystallographic parameters** | | | | | | **Atomic Position** | | | | **Bond Length (Å)** | | | |
|---|---|---|---|---|---|---|---|---|---|---|---|---|---|
| **Axis (Å)** | | | **Angle (degree)** | | | **atom** | **x** | **y** | **z** | **Calculated value of Zr atom with** | | **Compared with refrence value of Zr atom [3].** | |
| **a** | **b** | **c** | $\alpha$ | $\beta$ | $\gamma$ | | | | | **O1** | **O2** | **O1** | **O2** |
| 5.169 | 5.232 | 5.341 | 90 | 99.25 | 90 | Zr | 0.2758 | 0.0404 | 0.2089 | 2.1070 | 2.2634 | 2.1070 | 2.2634 |
| | | | | | | O1 | 0.6090 | 0.3420 | 0.3450 | | | | |
| | | | | | | O2 | 0.4510 | 0.7850 | 0.4790 | | | | |

Table 4.2 Illustrates lattice parameters and atomic position of Fe and O in $\alpha$-$Fe_2O_3$ polymorphs.

| **Crystallographic parameters** | | | | | | **Atomic Position** | | | | **Bond Length (Å)** | |
|---|---|---|---|---|---|---|---|---|---|---|---|
| **Axis (Å)** | | | **Angle (degree)** | | | **atom** | **x** | **y** | **z** | **Calculated Fe atom with O** | **Compared with refrence value [11].** |
| **a** | **b** | **c** | $\alpha$ | $\beta$ | $\gamma$ | | | | | | |
| 5.038 | 5.038 | 13.772 | 90 | 90 | 120 | Fe | 0.0000 | 0.0000 | 0.3553 | 1.54000 | 1.54112 |
| | | | | | | O | 0.3059 | 0.0000 | 0.2500 | | |

# CONCLUSION

In this research two polymorphs material $\alpha$-$Fe_2O_3$ and $ZrO_2$ were studied in terms of their crystallographic characteristics. Crystal structure models of $\alpha$-$Fe_2O_3$ and $ZrO_2$ were visualized as polyhedral, wireframe, space filling and stick forms for better understanding of atomic models by using VESTA. Crystallographic representation in terms of fractional coordinates were also visualized by 3D structures and have studied their behavior in respective fractional coordinates. It also provides information about the position of atomic nuclei. Lattice planes were also drawn in $\alpha$-$Fe_2O_3$ and $ZrO_2$ crystal structures models by using VESTA software. Powder diffraction patterns (XRD) were also generated for $\alpha$-$Fe_2O_3$ and $ZrO_2$ by using VESTA. For $ZrO_2$ the highest peaks occur at plane of (111) while on the other hand $\alpha$-$Fe_2O_3$ shows highest peak at (104) plane. X-rays diffracted from these particular planes represents dominancy of these planes in $\alpha$-$Fe_2O_3$ and $ZrO_2$ crystal structure samples. The bond length of Zr and Fe atoms with different Oxygen atoms was estimated by using VESTA software. The bond lengths are calculated in Angstroms (Å). The bond length Between zirconium Zr and oxygen O1 was 2.1070 Å while bond length between Zr and O2 was 2.2634 Å. For Iron Fe and oxygen O the calculated bond length between them was 1.5400 Å and all the values were in good agreement with previously investigated values. This VESTA tool may be used to analyze various characteristics such as lattice planes, crystal structures, fractional coordinates, and electron/nucleus density for a variety of transition metal oxide polymorphs nanomaterials.

# LIMITATIONS

- Since VESTA is an open source software and it has its own limitations as compared to other paid advanced software like VASP and WIEN2K software.
- VESTA provides accurate values of crystal structure, electronic densities, nuclear densities and powder diffraction patterns of materials. But it does not provide information about electronic band structure of materials.

# RECOMMENDATIONS

- For better performance of structural analysis other parameters should also be optimized.
- In Future the proposed structures should be implemented experimentally.
- Crystal structures and other parameters can be used to compare the structures that are experimentally prepared to determine better structural analysis.

# REFRENCES


[1] Crystal Structure. Available from:

https://en.wikipedia.org/wiki/Crystal_structure [cited January9, 2021].

[2] Crystal Structure. Available from: https://chem.libretexts.org/Crystal structure [cited January 9,2022].

[3] Kumar, N; Singh, D; Kumar, P.; Gangwar, J. Crystallographic Representation of polymorphs $ZrO_2$ using VESTA software. *AIP Conference proceedings*, volume 2142(1), pg. 0011331 - 0011336 (2019).

[4] Oxides. Available from: https://en.wikipedia.org/wiki/Oxide [cited January 9,2022].

[5] Periodic table. Available from:

https://en.wikipedia.org/wiki/Periodic_table#:~:text=Today%2C%20118%20elements%20are%20known,of%20which%20occur%20in%20nature [cited January 10,2022].

[6] D Block Elements. Available from: https://byjus.com/jee/d-block-elements/ [cited January 10,2022].

[7] Electronic configuration and general properties of d-block elements [Internet]. Available from: https://onlinesciencenotes.com/electronic-configuration-and-general-properties-of-d-block-elements-or-transition-elements/ [cited January 12,2022].

[8] Iron. Available from: https://en.wikipedia.org/wiki/Iron [cited January12,2022].

[9] Allotropes of Iron. Available from: https://en.wikipedia.org/wiki/Allotropes_of_iron [cited January12,2022].

[10] Iron (III) Oxide. Available from: https://en.wikipedia.org/wiki/Iron_oxide#:~:text=Iron%20oxides%20are%20chemical%20compounds%20composed%20of%20iron%20and%20oxygen.&text=Iron%20oxides%20are%20inexpensive%20and,it%20has%20E%20number%20E172. [cited January12,2022].

[11] Siroha, P.; Singh, D.; Soni, R.; Gangwar, J. Comparative Study on Crystallographic Representation of Transition Metal Oxides Polymorphs Nanomaterials using VESTA Software: Case Study on $Fe_2O_3$ and $TiO_2$. *AIP Conference proceedings*, volume 2006(1), pg. 030038 (2018).

[12] Machala, L.; Tucek, J.; Zboril, R. Polymorphous transformations of nanometric iron (III) oxide: a review. *Chemistry of Materials*, volume 23(14), pg. 3255-72 (2011).

[13] Tucek, J.; Zboril, R.; Namai, A.; Ohkoshi, SI. ε-$Fe_2O_3$: An advanced nanomaterial exhibiting giant coercive field, millimeter-wave ferromagnetic resonance, and magnetoelectric coupling. *Chemistry of Materials*, volume 22(24), pg. 6483-505 (2010).

[14] Lin, YF.; Liang, FL. Synthesis of a $ZrO_2$/carbon aerogel composite with tetragonal $ZrO_2$ structures assisted by the formation of phenol formaldehyde resin. *CrystEngComm*, volume 17(3), pg. 678-85 (2015).

[15] Zirconium Wikipedia Available from: https://en.wikipedia.org/wiki/Zirconium [cited April 1,2022].

[16] Crystallography. Available from:

https://www.britannica.com/science/crystallography [cited January13,2022].

[17] Terki, R; Bertrand, G; Aourag, H; Coddet, C. Structural and electronic properties of zirconia phases: A FP-LAPW investigations. *Materials science in semiconductor processing*, volume9(6) pg.1006-13 (2009).

[18] Crystallography & Types of Crystals. Available from: https://schoolworkhelper.net/crystallography-types-of-crystals/ [cited January13,2022].

[19] Yamin, M.; Islam, M.; Farooq, M. Physics Subjective. Physics of Solids, New Revised Edition (2017-2018), Muhammad Shahid Qureshi and Scholar Publications Urdu bazar Lahore, pages (1-437), 2008.

[20] X-ray diffraction analysis. Available from:

https://www.twi-global.com/technical-knowledge/faqs/x-ray-diffraction#:~:text=X%2Dray%20diffraction%20analysis%20(XRD)%20is%20a%20technique%20used,leave%20the%20material%20%5B1%5D. [cited April30,2022].

[21] Powder X-ray Diffraction. Available from: https://chem.libretexts.org/Bookshelves/Analytical_Chemistry/Supplemental_Modules_(Analytical_Chemistry)/Instrumental_Analysis/Diffraction_Scattering_Techniques/Powder_Xray_Diffraction#:~:text=In%20powder%20X%2Dray%20diffraction,require%20individual%20crystals%20be%20made [cited Feburary22,2022].

[22] X-ray Powder Diffraction (XRD). Available from: https://serc.carleton.edu/research_education/geochemsheets/techniques/XRD.html [cited Feburary22,2022].

[23] Applications and Principles of X-ray crystallography. Available from: https://www.azom.com/article.aspx?ArticleID=18684 [cited Feburary22,2022].

[24] Purnamasari, I.; Farida, I.; Nanang, N.; Zhafirah, A. Crystal structure analysis of Lanthanum Orthoferrite doped Zirconium with sol-gel method for solar cell candidate. *In Journal of Physics: Conference Series*, volume. 1869(1), pg. 012197 (2021).

[25] Kumar, D.; Singh, A.; Kaur, N.; Thakur, A.; Kaur, R. Tailoring structural and optical properties of ZrO2 with nickel doping. *SN Applied Sciences*, volume 2(4), pg.1-8 (2020).

[26] Amita, Asha.; Vishakha, Neetu.; Singh, D.; Kumar, N.; Kumar, R.; Gangwar, J. Crystallographic representation of Patterson densities of polymorphs α-$Fe_2O_3$. *AIP Conference Proceedings*, Volume 2220(1), pg. 020173 (2020).

[27] Cursaru, LM.; Piticescu, RM.; Dragut, DV.; Tudor, IA.; Kuncser, V.; Iacob, N.; Stoiciu, F. The influence of synthesis parameters on structural and magnetic properties of iron oxide nanomaterials. *Nanomaterials*, volume10(1), pg. 85 (2020).

[28] Ounacer, M.; Essoumhi, A.; Sajieddine, M.; Razouk, A.; Costa, BF.; Dubiel, SM.; Sahlaoui, M. Structural and magnetic studies of annealed iron oxide nanoparticles. *Journal of Superconductivity and Novel Magnetism*, volume 33(10), pg. 3249-61 (2020).

[29] Ghosh, A.; Srinivas, V.; Sundara, R. Comprehensive structural and magnetic properties of iron oxide nanoparticles synthesized through chemical routes. *Journal of Alloys and Compounds*, volume 818, pg. 152931 (2020).

[30] Kershi, RM.; Ali, FM.; Sayed, MA. Influence of rare earth ion substitutions on the structural, optical, transport, dielectric, and magnetic properties of superparamagnetic iron oxide nanoparticles. *Journal of Advanced Ceramics*, volume 7(3), pg.218-28 (2018).

[31] Sans, JA.; Monteseguro, V.; Garbarino, G.; Gich, M.; Cerantola, V.; Cuartero, V.; Monte, M.; Irifune, T.; Muñoz, A.; Popescu, C. Stability and nature of the volume collapse of ε-$Fe_2O_3$ under extreme conditions. *Nature communications*, volume9(1), pg.1-11 (2018).

[32] McKenna, KP.; Hofer, F.; Gilks, D.; Lazarov, VK.; Chen, C.;Wang, Z.; Ikuhara, Y. Atomic-scale structure and properties of highly stable antiphase boundary defects in $Fe_3O_4$. *Nature communications*, volume 5(1), pg.1-8 (2014).

[33] Ohgi, Y.; Ishihara, A.; Matsuzawa, K.; Mitsushima, S.; Ota, KI.; Matsumoto, M.; Imai, H. Factors for improvements of catalytic activity for zirconium oxide-based oxygen-reduction electrocatalysts. *ECS Transactions*, volume 41(1), pg. 162-167 (2011).

[34] Ding, J.; Fan, T.; Zhang, D.; Saito, K.; Guo, Q. Structural and optical properties of porous iron oxide. *Solid state communications*, volume 151(10), pg. 802-5 (2011).

[35] Zhen, G.; Muir, BW.; Moffat, BA.; Harbour, P.; Murray, KS.; Moubaraki, B.; Suzuki, K.; Madsen, I.; Agron-Olshina, N.; Waddington, L.; Mulvaney, P. Comparative study of the magnetic behavior of spherical and cubic superparamagnetic iron oxide nanoparticles. *The Journal of Physical Chemistry C*, volume 115(2), pg. 327-34 (2011).

[36] VESTA JP Minerals. Available from: https://jp-minerals.org/vesta/en/ [cited Feburary22,2022].

5/10/2022 Turnitin

Physics

About this page

This is your assignment inbox. To view a paper, select the paper's title. To view a Similarity Report, select the paper's Similarity Report icon in the similarity column. A ghosted icon indicates that the Similarity Report has not yet been generated.

## BA/BSc June Defense 2022

## Inbox | Now Viewing: new papers ▼

Submit File Online Grading Report | Edit assignment settings | Email non-submitters

Delete | Download | move to...

| | Author | Title | Similarity | web | publication | student papers | Grade | response | File | Paper ID | Date |
|---|---|---|---|---|---|---|---|---|---|---|---|
| | Zainab Nasir | BA/BSC JUNE DEFENSE 2022 | 12% 12% | 5% | 9% | 2% | | | download paper | 1831850990 | 09-May-2022 |
| | Maha Javed | BA/BSC JUNE DEFENSE 2022 | 16% 16% | 9% | 11% | 3% | | | download paper | 1831943702 | 09-May-2022 |
| | Maria Aisar | BA/BSC JUNE DEFENSE 2022 | 17% 17% | 11% | 8% | 8% | | | download paper | 1831945134 | 09-May-2022 |
| | Noor-ul-ain | BA/BSC JUNE DEFENSE 2022 | 17% 17% | 9% | 12% | 6% | | | download paper | 1831948114 | 09-May-2022 |